Intense laser field ionization of atom and molecular ion

by

Zi Jian Long

A thesis
presented to the University of Waterloo
in fulfilment of the
thesis requirement for the degree of
Master of Science
in
Physics

Waterloo, Ontario, Canada, 2008

AUTHOR'S DECLARATION FOR ELECTRONIC SUBMISSION OF A THESIS

I hereby declare that I am the sole author of this thesis. This is a true copy of the thesis, including any required final revisions, as accepted by my examiners.

I understand that my thesis may be made electronically available to the public.

Abstract

In order to understand how does the intense laser interact with matter we first of all study the ionization process. In this highly nonlinear region the conventional perturbation theory will fail to predict the experimental results. Alternative theories have been proposed in the past few decades. The fundamental difficulty in these new approaches is when laser field becomes so intense such that it is comparable to the Coulomb field at where the ground state electron mainly concentrate, we have to treat the laser field and the Coulomb field on an equal footing. The analytical solution that can describe the propagation of electron in both the laser field and the Coulomb field has not been found; therefore, in these new theories the ionization process is either divided temporarily into laser period and Coulomb period or spatially into laser field domain and Coulomb field domain. The propagation of electron in the full Hamiltonian is avoided.

In this thesis we study the intense field ionization process through both the analytical and numerical methods. For the analytical study we start with the intense field many-body S-matrix theory (IMST) [5] and integrate the direct electron term (it is the first term of the expansion in IMST) using saddle point method in the asymptotic region where the Keldysh parameter $\gamma \ll 1$. In addition, The tunneling ionization and multi-photon ionization as two different ionization regions are discussed.

We also study the ionization of one dimensional hydrogen atom and H_2^+ ion. Through numerically solving the time dependent Schrödinger equation (TDSE), we investigate the effects of laser pulse length, intensity and carrier envelope phase (CEP) on the photoelectron spectra. This study will help us understanding the dynamics of electron during ionization process. Moreover, the spectra calculation through numerical integration of direct electron term is carried out. Comparing the spectra with TDSE spectra allow us to test the validity of strong field approximation (SFA). In the case of H_2^+ ion we focus on the internuclear separation dependency of the photoelectron spectra. The polarization effect is discussed and some comparisons with H atom are carried out.

Acknowledgements

I am very grateful to Professor Wing-Ki Liu, for his patient supervision and encouragement. He spent hours and hours in correcting my thesis and then explained to me the proper way to write my thesis. He always encouraged me to participate in conferences so that I can have a broader view in my field of research. I have obtained solid training in mathematics and gained deep insight in atomic and molecular physics from Prof. Liu.

I also want to give thanks to my friends. Without them, I will not have the motivation to complete my study.

I am also very grateful to my Examining Committee members, Professor Joseph Sanderson and Professor Li Wei. They read my thesis carefully and gave many good suggestions on my work.

Contents

List of Figures

Chapter 1

Introduction

1.1 Light-Matter interaction

The development of physics sometimes can be summarized according to the attainability of one particular physical parameter. The intensity of light is one such example. Before the invention of laser, the intensity is low so that perturbation theory is sufficient to describe its interaction with matter. Based on this theory, conventional spectroscopy has long been used to study the material structure because weak field will drive transitions between atomic/molecular states without much distortion of the material itself. The well-known photo-electric effect is observed only if photon energy is above the ionization threshold, and the effect is independent of light intensity. However after the laser is invented it is possible to achieve higher intensities. Nonlinear optical effects were discovered so that electrons can absorb more than one photon during the transition. New phenomena such as second harmonic generation and Raman scattering emerged and found very important applications. Recently scientists have endeavored to compress the laser pulse length to the order of femtoseconds thus generating light with unprecedented high intensity. When these pulses interact with atoms or molecules many new phenomena will appear. Even with photon energy much smaller than the ionization threshold it is possible to ionize the atom/molecule by absorption of a large number of photons, making a direct transition from a bounded state to the continuum. Above threshold ionization (ATI) discovered in 1979 by Agostini [29], demonstrated that it is possible for the atom

to absorb more photons than the minimum required for ionization. The photo-electron spectra show distinct peaks separated by exactly one photon energy. Another example is the high harmonic generation (HHG), the emission of photon observed at frequencies that are high multiples of the laser frequency. The spectrum can even reach the extreme ultra-violate (XUV) region. Most importantly, as the pulse length gets shorter, the motion of the electron is not due to the accumulation of many cycles of the electric field but is controlled by a few cycle of oscillations. Consequently the dynamics is sensitive to the carrier-envelope phase (CEP) [36]. This implies that for ultra-short and intense laser pulses, it is possible to control the electron dynamics by shaping the pulse, and use this well-controlled electron to image the atom and molecule or to probe the parent ion dynamics [16, 26].

The size of atom is on the order of the Bohr radius a_0 and the classical orbiting period of the valence electron can be defined as $\omega_{atom} = \frac{I_p}{\hbar}$. The atomic electric field $E_{atom} = \frac{e}{4\pi\varepsilon_0}\frac{1}{a_0^2}$, with the corresponding field intensity $I_{atom} = \frac{1}{2}c\varepsilon_0 E_{atom}^2$. For a hydrogen atom the electron will go around the core 3×10^{15} times in one second. E_{atom} is equal to $5.4\times10^{11} V/m$ or one atomic unit (a.u. see Appendix A). I_{atom} is equal to $3.5\times10^{16} W/cm^2$ or 5.45 a.u. For a laser pulse in the infrared region the wave length is about 900 nm. The pulse length can be so short that it only contains a few cycles of the electric field oscillation. The intensity of the laser pulse will be so high such that at the peak of the laser pulse, the electric field strength is comparable to the atomic electric field strength. At this intensity, the electron will be easily set free and then driven by the external electric filed oscillating in the vicinity of the parent ion (usually smaller than laser wave length). Inelastic collision with the ion may occur and the electron will either recombine with the core generating high harmonic radiation, or it will knock out another electron. The subsequent dynamics could be very complicated and it is important to understand how the electron become ionized at the first place.

1.2 Classification of ionization

Ionization from the conventional point of view is divided into two regimes: tunneling ionization and multiphoton ionization. If the photon energy is much smaller than the ionization potential and the peak electric field strength of laser approaching the atomic electric

field strength then the electron will have significant probability of tunneling through the potential barrier. Keldysh [20] defined a parameter to characterize this region as the ratio of the laser frequency ω_L to the tunneling frequency ω_t:

$$\gamma = \frac{\omega_L}{\omega_t} = \frac{\omega_L \sqrt{2I_p}}{E_0} \tag{1.1}$$

where the $\omega_t = \frac{E_0}{\sqrt{2I_p}}$ [17]. Here ω_L is the laser frequency, I_p is the ionization potential and E_0 is the maximum electric field of the laser. The atomic units are used (see Appendix A). γ can also be expressed as:

$$\gamma = \sqrt{\frac{I_p}{2U_p}}$$

where $U_p = \frac{E_0^2}{4\omega_L^2}$ is the pondermotive potential or the time-averaged quiver energy of a free-electron in the laser field [8]. When γ is much less than unity then the ionization will be mainly due to tunneling. This tunneling ionization is based on a static point of view of the system. In this case the energy of electron does not change significantly from the ground state energy but the energy level is broadened (i.e. it becomes a quasi-static state), so that the electron has finite probability to tunnel through the potential barrier set up by the Coulomb potential and the electric field of laser. After tunneling the electron will appear in the continuum with zero kinetic energy and thereafter will be accelerated by the external electric field of the laser. When Keldysh parameter is greater than one, the laser frequency is comparable to the electron orbiting frequency and the electron couples to the continuum through multi-photon absorption. ATI spectrum can be viewed as a signature of this process. The oscillating electric field drives the bounded electron and creates a train of outgoing electron pulses; these pulses will interfere with each other and form the ATI spectrum. Attempts have been made to find a more precise definition of these two ionization channels [15, 17, 37]. In the transition region where the Keldysh parameter is close to one, the tunneling and multi-photon ionization both have contributions.

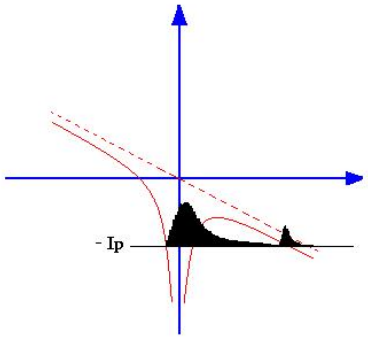

Figure 1.1: The applying electric field is so strong such that the Coulomb potential is greatly distorted. The resultant potential forms a barrier with finite width for the ground state electron to tunnel through. Note the energy level of electron is assumed to be unchanged after the external field is applied.

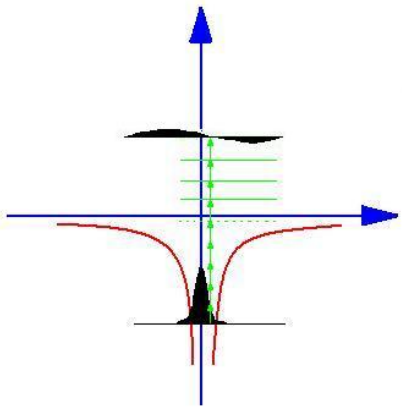

Figure 1.2: The electron will be kicked into continuum by the laser field. Once it appears in the continuum its propagation will be dominated by the laser field because the free electron wave function extends to a larger area in space where the Coulomb field is negligible compare with the intense laser field.

1.3 Theoretical approaches to the intense field ionization.

As the laser intensity increases, conventional perturbation theory becomes inappropriate to address the ionization problem because there are large numbers of atomic states coupled in the process. One commonly-used formula to calculate ionization probability is derived by Ammosov, Delone, and Krainov (ADK) [1], based on the tunneling theory of Landau and Lifshitz, Smirnov, and Chibisov, Perelomov, Popov, and Terentev [30, 33, 25]. The idea is to view the external field as a static electric field, so that the bounded electron sees a potential barrier with finite width. Thus the electron will have some probability to tunneling through that potential barrier (Figure 1.1). The calculation starts from the time independent Schrödinger equation for a hydrogen atom in a static electric field, and the exponential decay factor inside the barrier is found by the WKB approximation (see Appendix B). To account for the time variation of the laser field, the ionization rate is averaged over time without considering the interference of the transition amplitude [30]. For a complex atom the many-electron effect is taken into account by introducing an effective quantum number [1]; a more pedagogical derivation is given in recent paper [6]. This formula is proven to be useful to interpret experimental results [2, 37]. Note that in the region close to the atomic core the wave function is assumed to be the atomic wave function, and within the barrier the Coulomb potential is treated as small quantity in order to evaluate the WKB integral. The leading term will give rise to the tunneling exponential factor while the first order term will give rise to the pre-exponential coefficient. Thus space is actually divided into a region dominated by the Coulomb field and a region dominated by the laser field.

A more general approach was given in 1964 by Keldysh [20]. He proposed the strong field approximation (SFA) which assumes that initially the electron is in the ground state of the atomic field; at later times the laser field will pump the electron into the continuum and then drives this electron oscillating in space with the atomic field neglected (Figure 1.2). The ATI spectrum can be explained very well by this theory in the case of short-range potential. But as we will see in Chapter 3 for a long-range potential, The SFA does not work very well. However, the strong field approximation is the only practical approach besides exact numerical integration of the Schrödinger equation. One of our

goals in this thesis is to examine this approximation by comparing it with exact numerical calculations for a one-dimensional model with long range potential.

Under high laser intensity, a semi-classical three step model has been used to describe the electron dynamics and was extensively verified [10, 27]. The model assumes that initially the electron appears in the continuum at time t_i with negligible kinetic energy and subsequentlly be driven away by the electric field. When the electric field changes direction the electron will then be pulled back and recollide with the parent ion. The recollision process will give rise to high harmonic generation and double ionization [32]. We have not considered these problems in this thesis. The importance of the first two steps is obvious. The ADK ionization rate has been used to weigh the interaction time and propagates the classical electron in time results a photoelectron spectrum [9].

The ADK formula has been generalized to diatomic molecules [38]. This generalization includes expanding the initial molecular wave function in a linear combination of one-center spherical harmonics and summing the ADK ionization rate for each harmonics to give the total ionization rate. This method takes into account the symmetry of molecular orbital and explains some espect of the ionization suppression.

Becker and Faisal introduced the intense field many-body S-matrix theory [12]. They used the language of scattering matrix to incorporate Keldysh's original postulate into a modified expansion of the transition matrix. In this theory the SFA corresponds to a truncation of the infinite series. A more detailed discussion of this general formalism is discussed in the next chapter.

1.4 Our purpose and questions remaining

Since a complete analytical solution of the Schrödinger equation with the presence of both atomic potential and laser field has not been found, we have to either work with the atomic wave functions or Volkov wave function as basis (see Chapter 2 and Appendix C). Conventional perturbation theory takes the atomic basis as reference states because the laser interaction is assumed to be weak compared to the Coulomb field. However when the laser field is strong, the number of atomic states involved in the the ionization process becomes very large, and perturbation theory fails to explain the experimental results. Our

purpose is to study the non-perturbative theories proposed in the past few decades. We will especially focus on the intense field many-body scattering matrix theory [5], and derive an ADK-type formula using the SFA. Through a simple one-dimensional model we study various phenomena in the intense field ionization process. Also the validity of the strong field approximation will be tested.

1.5 Organization of the thesis

In Chapter 2 we will first introduce the intense field many-body scattering matrix theory and describe the direct electron term. We then use the saddle point method to integrate this term. In the tunneling region we obtain a compact formula for total ionization rate. In Chapter 3, one-dimensional models for the H atom and the H_2^+ ion are introduced and both numerical solution of the time-dependent Schrödinger (TDSE) and SFA calculations are carried out. In Chapter 4, we present the conclusion of this thesis.

Chapter 2

Theory

A widely used theoretical approach to calculate intense field ionization rate is the scattering matrix formalism. This intense field many body S-matrix theory (IMST) was introduced by Becker and Faisal [5] which provides a systematic expansion of the transition amplitude in a series involving various interactions of the system. We will concentrate on the first term of this series, the direct electron term, to show that it is possible to derive an ADK-type tunneling ionization rate formula. When the pondermotive potential U_p is very large compare to the photoelectron energy, the saddle point approximation can be applied in the asymptotic region. We will see that the Keldysh parameter appears naturelly when we carry out the integration analytically. We show that the saddle point approximation has a close connection to the adiabatic approximation.

2.1 Single active electron in laser field (SAE)

The strong field ionization process for an atom or molecule can be well described by assuming one active electron experiencing an effective potential $\hat{V}_a$ formed by the nucleus and other electrons [24, 5]. In the presence of EM fields, the Schrödinger equation can be written as

$$i\hbar\frac{\partial}{\partial t}\Psi = \frac{1}{2m_e}\left[\hat{P} + e\vec{A}(\vec{r},t)\right]^2\Psi + \hat{V}_a(\vec{r})\Psi - e\Phi_L(\vec{r},t)\Psi, \tag{2.1}$$

where the charge of the electron is $-e$ ($e > 0$), and $\hat{P} = -i\hbar\nabla$ is the linear momentum operator for the electron. $\vec{A}(\vec{r}, t)$, $\Phi_L(\vec{r}, t)$ are the vector and scalar potentials from which the electric and magnetic field can be obtained as [18]:

$$\vec{E} = -\nabla\Phi_L - \frac{\partial}{\partial t}\vec{A} \tag{2.2}$$

$$\vec{B} = \nabla \times \vec{A}. \tag{2.3}$$

As is well known, these potentials are not unique. Any gauge transformation with the following form will not affect the physical observables $\vec{E}$ and $\vec{B}$:

$$\Phi'_L(\vec{r}, t) = \Phi_L(\vec{r}, t) - \frac{\partial}{\partial t}\chi(\vec{r}, t) \tag{2.4}$$

$$\vec{A}'(\vec{r}, t) = \vec{A}(\vec{r}, t) + \nabla\chi(\vec{r}, t) \tag{2.5}$$

where $\chi(\vec{r}, t)$ is an arbitrary differentiable real function. The corresponding wave functions are related by a phase factor [7]:

$$\Psi' = \Psi \exp[-ie\frac{\chi}{\hbar}]. \tag{2.6}$$

Therefore it is possible to choose a specific gauge such that $\nabla \cdot \vec{A} = 0$. This is defined as the Coulomb gauge. In free space where no sources are present, the scalar potential $\Phi_L = 0$ and the vector potential satisfies the wave equation [18]:

$$\nabla^2\vec{A} - \frac{\partial^2}{\partial t^2}\vec{A} = 0.$$

Hence equation (2.1) can be rewritten as:

$$i\hbar\frac{\partial}{\partial t}\Psi = \left[\frac{1}{2m_e}\hat{P}^2 + \frac{e}{m_e}\vec{A}(\vec{r}, t) \cdot \hat{P} + \frac{e^2}{2m_e}A^2(\vec{r}, t)\right]\Psi + V_a(\vec{r})\Psi. \tag{2.7}$$

When the laser wave length is much larger than the size of the system and the intensity of laser is not so strong such that the photo-electron speed is much less than the speed of light, we can introduce the dipole approximation and assume the field is uniform across the spatial extent of interest:

$$\vec{A}(\vec{r}, t) \approx \vec{A}(t). \tag{2.8}$$

The A^2 term inside the square bracket of eq.(2.7) then becomes a function of time only. It can be eliminated through the transformation:

$$\Psi^v = \Psi \exp\left(\frac{ie^2}{2m_e^2}\int^t A^2 dt\right) \tag{2.9}$$

After the transformation, equation (2.7) becomes:

$$i\hbar\frac{\partial}{\partial t}\Psi^v = \left[\frac{1}{2m_e}\hat{P}^2 + \frac{e}{m_e}\vec{A}(t)\cdot\hat{P}\right]\Psi^v + \hat{V}_a(\vec{r})\Psi^v \tag{2.10}$$

This is referred as the velocity gauge (VG). The laser field is described by vector potential and couples to the wave function through the momentum operator. Another commonly-used gauge is called the length gauge (LG). It can be achieved through the gauge transformation (2.4). by choosing $\chi(\vec{r},t) = -\vec{r}\cdot\vec{A}(t)$ and define

$$\Psi^\ell = \exp(\frac{ie}{\hbar}\vec{r}\cdot\vec{A})\Psi. \tag{2.11}$$

We then obtain

$$i\hbar\frac{\partial}{\partial t}\Psi^\ell = \left[\frac{1}{2m_e}\hat{P}^2 + e\vec{r}\cdot\vec{E}(t)\right]\Psi^\ell + V_a(\vec{r})\Psi^\ell \tag{2.12}$$

In the length gauge, the laser field couples to the wave function through the position operator.

For a free electron with momentum $\vec{p} = \hbar\vec{k}$ in an EM field, the Schrödinger equation is given by eq.(2.10) in the velocity gauge or eq.(2.12) in the length gauge with $\hat{V}_a = 0$. The corresponding solutions are [7] called the Volkov solutions. The solution to eq.(2.10) is [7]

$$\Psi^v_{\vec{k}} = \exp\left(i\vec{k}\cdot\vec{r} - i\hbar\frac{k^2}{2}t\right)\exp\left(-i\vec{k}\cdot\int^t dt'\vec{A}(t')\right), \tag{2.13}$$

yielding the solution in Coulomb gauge

$$\Psi_{\vec{k}} = \exp\left(i\vec{k}\cdot\vec{r}\right)\exp\left(-\frac{i}{2m_e\hbar}\int^t dt'[\vec{p} + e\vec{A}(t')]^2\right), \tag{2.14}$$

from which the solution in the length gauge is obtained from (2.11)

$$\Psi^\ell_{\vec{k}} = \exp\left[i(\vec{k}\cdot\vec{r} + \frac{e}{\hbar}\vec{A}(t))\right]\exp\left(-\frac{i}{2m_e\hbar}\int^t dt'[\vec{p} + e\vec{A}(t')]^2\right). \tag{2.15}$$

Derivation of these solutions using Kramers-Henneberger transformation is given in Appendix C.

2.2 S-matrix expansion

In this section we follow Becker and Faisal [5] to derive an expansion of the transition amplitude for ionization. From now on we shall use atomic units in which $e = 1$, $m_e = 1$, $\hbar = 1$ and the Bohr radius $a_0 = 1$ (see Appendix A). The Hamiltonian for the single active electron can be written as

$$\hat{H} = \hat{T} + \hat{V}_a + \hat{V}_L. \tag{2.16}$$

Where $\hat{T} = -\frac{1}{2}\nabla^2$ is the kinetic energy operator and $\hat{V}_L$ is the electron-laser interaction given by

$$\hat{V}_L = \vec{A} \cdot \hat{P}$$

in the velocity gauge of eq. (2.10) or

$$\hat{V}_L = \vec{r} \cdot \vec{E}$$

in the length gauge of eq. (2.12). Therefore the Hamiltonian can be partitioned in two different ways. In one way we have

$$\hat{H} = \hat{H}_a + \hat{V}_L \tag{2.17}$$

where $\hat{H}_a = \hat{T} + \hat{V}_a$ is the Hamiltonian of the atom or molecule in the absence of the laser. Another way is to write

$$\hat{H} = \hat{H}_L + \hat{V}_a \tag{2.18}$$

where $\hat{H}_L = \hat{T} + \hat{V}_L$ is the Hamiltonian of a free electron in the presence of the laser. Initially the system is in the bound state $\phi_i(t)$ governed by $\hat{H}_a$:

$$i\frac{\partial}{\partial t}\phi_i(t) = \hat{H}_a\phi_i(t). \tag{2.19}$$

After ionization the system will be described by the state $\psi_f(t)$ of $\hat{H}_L$:

$$i\frac{\partial}{\partial t}\psi_f(t) = \hat{H}_L\psi_f(t). \tag{2.20}$$

In the presence of the laser, the wave function can be split into two parts

$$\Psi(t) = \phi_i + \Psi'(t). \tag{2.21}$$

Using the partition equation (2.17) and substituting equations (2.19) and (2.21) into the time dependent Schrödinger equation

$$i\frac{\partial}{\partial t}\Psi = \hat{H}\Psi,$$

we obtain:

$$(i\frac{\partial}{\partial t} - \hat{H})\Psi'(t) = \hat{V}_L\phi_i(t). \tag{2.22}$$

The above differential equation can be transformed into an integral equation by introducing the Green's function

$$(i\frac{\partial}{\partial t} - \hat{H})G(t,t') = \delta(t-t') \tag{2.23}$$

and considering the right hand side as a source term, yielding

$$\Psi'(t) = \int_{t_i}^{t_f} dt' G(t,t')\hat{V}_L(t')\phi_i(t') \tag{2.24}$$

where the laser is turned on between t_i and t_f. The Green's function can be expanded using the partition of Hamiltonian in equation (2.18).

$$G(t,t') = G_L(t,t') + \int_{t_i}^{t_f} dt'' G_L(t,t'')\hat{V}_a G(t'',t') \tag{2.25}$$

where

$$(i\frac{\partial}{\partial t} - \hat{H}_L)G_L(t,t') = \delta(t-t'). \tag{2.26}$$

We can substitute equation (2.25) into equation (2.24) and obtain

$$\begin{aligned}\Psi'(t) &= \int_{t_i}^{t_f} dt' G_L(t,t')\hat{V}_L(t')\phi_i(t') \\ &\quad + \int_{t_i}^{t_f} dt'' \int_{t_i}^{t_f} dt' G_L(t,t'')\hat{V}_a G(t'',t')\hat{V}_L(t')\phi_i(t').\end{aligned} \tag{2.27}$$

The Green's function $G_L(t', t)$ can be written in the proper state of representation:

$$G_L(t, t') = -i\Theta(t - t') \sum_k |\psi_k^v(t)\rangle\langle\psi_k^v(t')| \tag{2.28}$$

where $\psi_k^v(t)$ is the Volkov solution for $\hat{H}_L$:

$$i\frac{\partial}{\partial t}\psi_k^v(t) = \hat{H}_L\psi_k^v(t).$$

Here the Heaviside function $\Theta(t - t')$ appears because of causality. It can be verified directly that equation (2.28) satisfies equation (2.26). We define the transition amplitude as:

$$\begin{aligned}(S-1)_{fi} &= \langle\psi_f(t_f)|\Psi(t_f) - \phi_i(t_f)\rangle \\ &= \langle\psi_f(t_f)|\Psi'(t_f)\rangle\end{aligned} \tag{2.29}$$

where $\psi_f(t_f)$ is one of the Volkov states in the expansion (2.28). We can combine equations (2.27)-(2.29) to obtain:

$$\begin{aligned}(S-1)_{fi} &= -i\int_{t_i}^{t_f} dt'\langle\psi_f(t')|\hat{V}_L(t')|\phi_i(t')\rangle \\ &\quad + \int_{t_i}^{t_f} dt'' \int_{t_i}^{t_f} dt'\langle\psi_f(t'')|\hat{V}_a G(t'', t')\hat{V}_L(t')|\phi_i(t')\rangle.\end{aligned} \tag{2.30}$$

The first term on right hand side is exactly the SFA matrix term proposed by Keldysh [20]. It is recognized as the direct electron term. Figure 2.1 illustrates the physical meaning of this term. The difference between the SFA and conventional perturbation theory, is that in conventional perturbation theory we constantly take the atomic states as reference states but in SFA we switch the reference states, to the Volkov states after ionization. This approximation is good for short range potentials [3, 14]. However in the case of long range potential such as the Coulomb potential the approximation can become inadequate when most of the time the electron will be confined in the region where the Coulomb field is still not negligible and it is necessary to take the second term of equation (2.30) into account. Further expansion of this term can be obtained

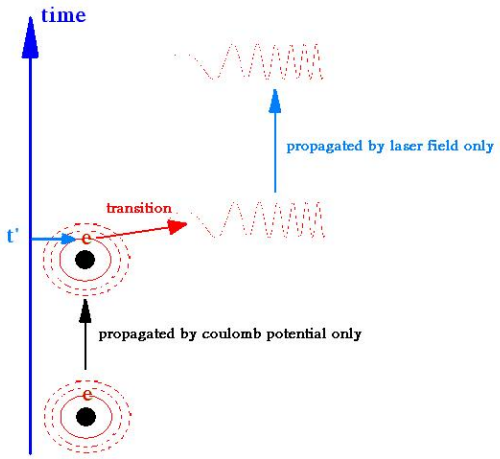

Figure 2.1: Initially the electron is in the atomic ground state. At some later time the laser field pumps the electron to an unbound state and then drives the electron oscillating back and forth. After the electron becomes free, it is assumed that the electron will not interact with the core again and the Coulomb potential is neglected. The population in the atomic excited states is neglected.

if we employ equation (2.27) again. Alternatively we can expand the Green's function according to the partition of the Hamiltonian in equation (2.17).

$$G(t,t') = G_a(t,t') + \int_{t_i}^{t_f} dt'' G_a(t,t'')\hat{V}_L(t'')G(t'',t')$$

This time the Green's function $G_a(t,t')$ is given by

$$\left(i\frac{\partial}{\partial t} - \hat{H}_a\right)G_a(t,t') = \delta(t-t').$$

The second term in equation (2.30) can be interpreted in terms of the re-scattering effects [5] but we do not study them in this thesis.

2.3 Analytical integration of the direct electron term

In the SFA, the transition amplitude $(S-1)_{fi}$ is approximated by the first term of eq. (2.30). We shall use the length gauge and identify $\psi_f(t)$ with the Volkov state eq. (2.17),

which in atomic unit is given by

$$\psi_f(\vec{r},t) = e^{i[\vec{k}+\vec{A}(t)]\cdot\vec{r}} e^{-\frac{i}{2}\int^t [\vec{k}+\vec{A}(t')]^2 dt'} \tag{2.31}$$

The interaction Hamiltonian is:

$$\hat{V}_L(t) = \vec{r}\cdot\vec{E}(t) = -\vec{r}\cdot\frac{\partial\vec{A}(t)}{\partial t} \tag{2.32}$$

The initial wave function is assumed to be the atomic or molecular ground state ϕ_g:

$$\phi_i(t) = \phi_g(\vec{r})e^{iI_p t} \tag{2.33}$$

where I_p is the ionization potential of the system. The transition amplitude becomes:

$$(S-1)_{fi}^{SFA} = -i\int_{t_i}^{t_f} dt \int d^3\vec{r}\exp\left[-i(\vec{k}+\vec{A}(t))\cdot\vec{r}\right]\vec{r}\cdot\vec{E}(t)e^{iS(t)}\phi_g(\vec{r})$$

where

$$S(t) = \frac{1}{2}\int^t [\vec{k}+\vec{A}(t')]^2 dt' + I_p t. \tag{2.34}$$

Recognizing

$$\frac{\partial}{\partial t}e^{-i[\vec{k}+\vec{A}(t')]\cdot\vec{r}} = -i\frac{\partial\vec{A}}{\partial t'}\cdot\vec{r}e^{-i[\vec{k}+\vec{A}(t')]\cdot\vec{r}} = i\vec{E}(t')\cdot\vec{r}e^{-i[\vec{k}+\vec{A}(t')]\cdot\vec{r}}$$

and integrating by parts, we obtain [28]

$$(S-1)_{fi}^{SFA} = \left[-\tilde{\phi}_g(\vec{k}+\vec{A}(t))e^{iS(t)}\right]_{t_i}^{t_f} + i\int_{t_i}^{t_f} dt\ \tilde{\phi}_g(\vec{k}+\vec{A}(t))S'(t)e^{iS(t)} \tag{2.35}$$

where

$$S'(t) = \frac{1}{2}(\vec{k}+\vec{A}(t))^2 + I_p, \tag{2.36}$$

and

$$\tilde{\phi}_g(\vec{k}) = \int d^3\vec{r}e^{-i\vec{k}\cdot\vec{r}}\phi_g(\vec{r}) \tag{2.37}$$

is the Fourier transform of the ground state wave function. For a ground state hydrogen atom [28]

$$\tilde{\phi}_g(\vec{k} + \vec{A}(t)) = \frac{(2I_p)^{\frac{5}{4}}}{\sqrt{2}\pi} \frac{1}{S'^2} \tag{2.38}$$

and the integral can be written as:

$$\frac{(2I_p)^{\frac{5}{4}}}{\sqrt{2}\pi} \left[\left[-\frac{1}{S'^2} e^{iS(t)} \right]_{t_i}^{t_f} + i \int_{t_i}^{t_f} dt \frac{e^{iS(t)}}{S'(t)} \right] \tag{2.39}$$

In order to integrate the above formula we extend the time variable to the complex plane. At high laser intensity the exponent is a rapidly varying function of t and the major contributions to eq.(2.39) comes from the vicinity of the saddle points located at $S'(t_s) = 0$. In the case of the Coulomb potential the integrand is not analytic at the saddle points; however by deviating the contour slightly from the saddle points we can still integrate using the saddle point method [28]. First of all let us take a look at the global topological structure of the integrand of (2.39) for the hydrogen atom in the complex time plane (see Figure 2.2). Along the real time axis, the integrand is a rapid oscillating function (see Figure 2.3). However after we deform the integration path to the upper complex plane the integrand only peaks at the saddle points, so that the integral in (2.39) can be expresses as.

$$i \int_{t_i}^{t_f} dt \frac{e^{iS(t)}}{S'(t)} = i \int_{a \to b} dt \frac{e^{iS(t)}}{S'(t)} + i \int_{b \to c} dt \frac{e^{iS(t)}}{S'(t)} + i \int_{c \to d} dt \frac{e^{iS(t)}}{S'(t)} \tag{2.40}$$

where a, b, c, d are the points in the complex time plane shown in Figure 2.5. The contributions to the integral are mostly concentrated at the saddle points for the new integration path $b \to c$. Note the laser period is 126 a.u. (labeled by a in Figure 2.3 and Figure 2.4). We can see from the Figure 2.4 that major contributions are located around the peaks of the electric field. The integrals $a \to b$ and $c \to d$ will cancel the the surface term in the eq. (2.39) [28]. The new integration path is deviated slightly from the original path because at the saddle points the integrand is not analytic and we should leave the singularities outside the contour (Figure 2.5). Following [28] we obtain the following formula:

$$(S-1)_{fi}^{SFA}(t_f, t_i) = (2I_p)^{\frac{5}{4}} \sum_s \frac{e^{iS(t_s)}}{S''(t_s)} \tag{2.41}$$

The saddle points in eq. (2.41) can be found by solving:

$$\frac{1}{2}(\vec{k} + \vec{A}(t))^2 + I_p = 0, \tag{2.42}$$

$$\vec{A}(t) = \vec{A}_o \sin(\omega_L t_s) \tag{2.43}$$

so that the electric field of the laser is given by $\vec{E}(t) = -\frac{\partial}{\partial t}\vec{A}(t) = \vec{E}_0 \cos\omega_L t$ where $\vec{A}_0 = -\frac{\vec{E}_0}{\omega_L}$. Denote the components of the momentum $\vec{k}$ of the photoelectron parallel and perpendicular to the laser polarization by $k_\parallel$ and $k_\perp$, respectively. Recall that the Keldysh parameter is given by $\gamma = \sqrt{\frac{I_p}{2U_p}}$ and define another parameter by $\beta = \frac{k_\parallel}{\sqrt{2U_p}}$. In the case of tunneling ionization, three conditions should be satisfied [20]:

$$\gamma \ll 1 \tag{2.44}$$

$$\beta \ll 1 \tag{2.45}$$

$$\frac{k_\perp^2}{2I_p} \ll 1 \tag{2.46}$$

corresponding to the physical situation of low frequency excitation and slow photoelectrons. We then obtain approximate solution of equation (2.43) :

$$\sin(\omega_L t_s) = -\beta \pm i\sqrt{2}\gamma \tag{2.47}$$

$$\cos(\omega_L t_s) = 1 + \gamma^2 - \frac{\beta^2}{2} \pm i\sqrt{2}\beta\gamma \tag{2.48}$$

$$t_s = (-\frac{\beta}{\omega_L} \pm i\sqrt{2}\frac{\gamma}{\omega_L}) + \frac{1}{6}(-\frac{\beta}{\omega_L} \pm i\sqrt{2}\frac{\gamma}{\omega_L})^3 \tag{2.49}$$

Substituting the above results into $S(t_s)$ and $S'(t_s)$ and keeping the leading order, we obtain

$$S''(t_s) = \pm\frac{\sqrt{I_p}k_\parallel}{\beta} \tag{2.50}$$

$$S(t_s) = \frac{U_p}{\omega_L}\left[-\frac{1}{3}\beta^3 - 2\beta\gamma^2 \pm i(\frac{15\sqrt{2}}{4}\beta^2\gamma + \frac{4\sqrt{2}}{3}\gamma^3)\right] \tag{2.51}$$

The ionization probability density is given by:

$$|(S-1)_{fi}^{SFA}(t_f, t_i)|^2. \tag{2.52}$$

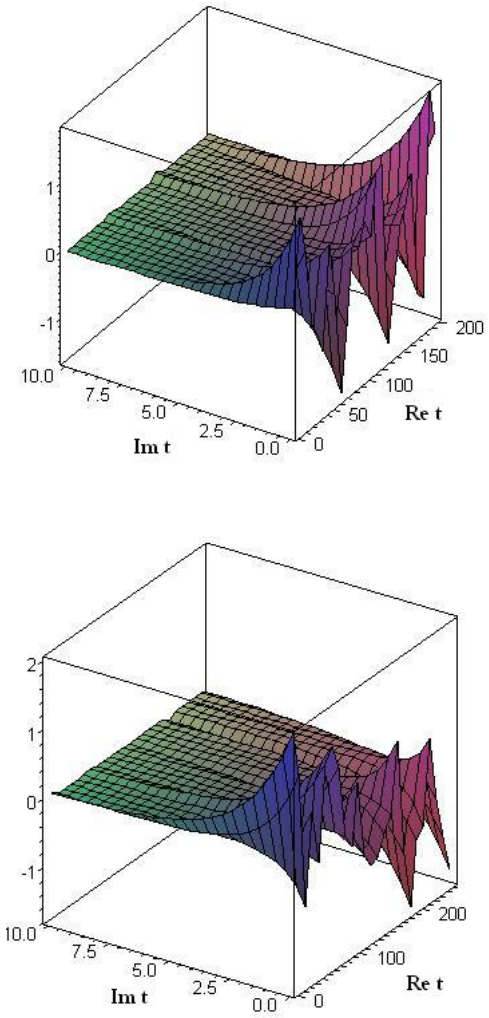

Figure 2.2: The global structure of the real (upper diagram) and imaginary parts (lower diagram) of the integrand in complex time plane. The $E_0 = 0.073$, $\omega_L = 0.05$ and $k = 0$, $I_p = 0.5$

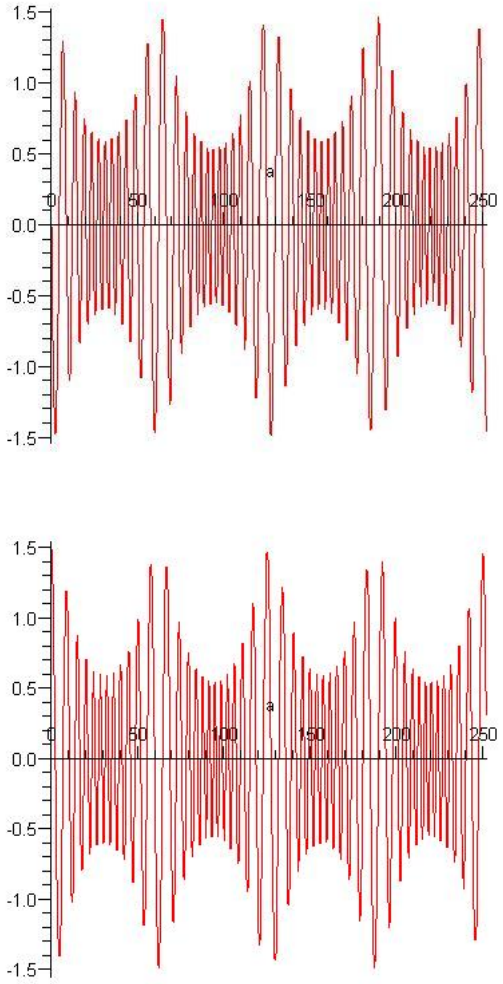

Figure 2.3: The real (upper diagram) and imaginary parts (lower diagram) of the integrand along the real time axis. The $E_0 = 0.073$, $\omega_L = 0.05$ and $k = 0$, $I_p = 0.5$

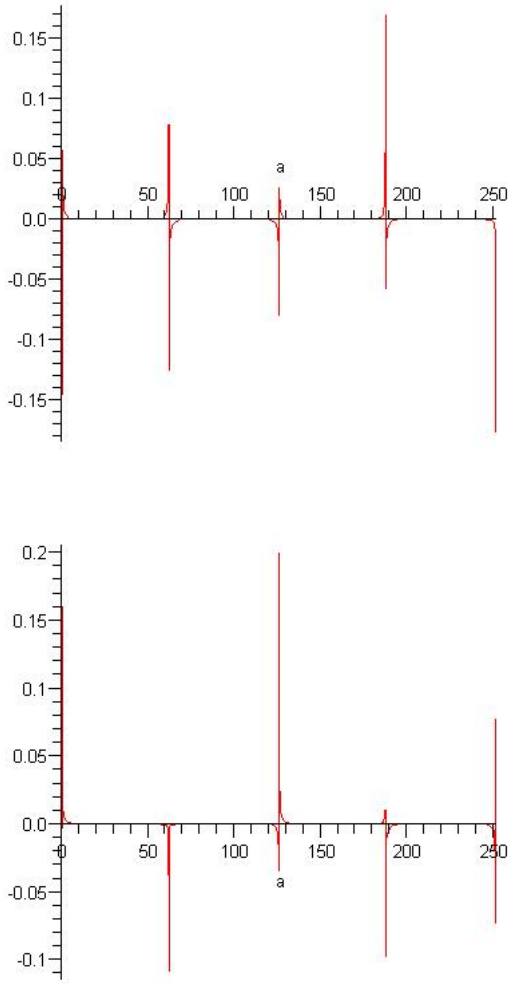

Figure 2.4: The real (upper diagram) and imaginary parts (lower diagram) of the integrand on deformed contour. The deformed contour is shown in Figure 2.5. The above graph corresponds to the path of $b \rightarrow c$ which gives the main contribution of transition amplitude.

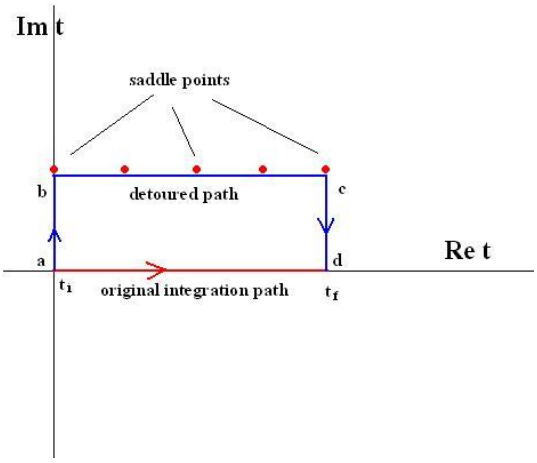

Figure 2.5: In the complex time plane the original integration path is deformed so that the new contour passes through the vicinities of the saddle points. Cauchy's integral theorem implies that the integral will have the same value for the path $t_i \to t_f$ and the path $t_i \to b \to c \to t_f$.

Neglecting the interference between saddle points, the total ionization rate is given by

$$\Gamma = \sum_s \int_0^\infty (2I_p)^{\frac{5}{2}} |\frac{e^{iS(t_s)}}{S''(t_s)}|^2 dk_\parallel \tag{2.53}$$

After some algebra we obtain an ADK-type tunneling ionization formula:

$$\Gamma = C_0 \frac{\omega_L}{(I_p)^{\frac{7}{2}}} \left(\frac{(2I_p)^{\frac{3}{2}}}{E_0} \right)^{\frac{3}{2}} e^{-\frac{2}{3}\frac{(2I_p)^{\frac{3}{2}}}{E_0}} \tag{2.54}$$

where C_0 is a constant related to the laser pulse length. The exponential factor is common to the tunneling of both long range and short range potentials. This factor can be considered as a character of tunneling ionization (see Appendix B). The pre-factor depends on some inverse power of the electric field strength. The power for short range potential is different from the power for long range potential. Here we only give the formula for the Coulomb potential.

2.4 The origin of the tunneling ionization

The direct electron term does not contain information of the potential barrier shape explicitly. However as we can see from last section, integrating the direct electron term in the asymptotic region will lead to a tunneling ionization formula. This is because the initial state ψ_i contains information of $\hat{V}_a$ implicitly. The Volkov state and the interaction Hamiltonian depend on the external electric field. When the inner product of eq. (2.29) is formed, the information of the potential barrier will be recovered; hence an ionization rate with the correct exponential factor is obtained. In SFA the ionization process is divided into two stages. In the first stage, the Coulomb field is dominant so that we can neglect the laser field. In the second stage the Coulomb field is neglected as the laser field dominates the ionized state. In ADK theory the space is divided into three regions. In the close core region, the laser field is neglected. In the far core region, the Coulomb field is negligible [17]. It is interesting to notice that both theories have to make this artificial division, but one in time and the other in space. The reason for this is because SFA is intrinsically a time-dependent theory so the ionization process is followed in time, while the ADK theory is a time-independent theory so the ionization process is described in space. When the electron tunnels through the potential barrier, its probability current flows from the close core region to the far core region, which corresponds to a transition from initial state ϕ_i to the continuous spectrum. In addition, tunneling ionization requires the Keldysh parameter $\gamma \ll 1$. This is actually the same criterion for the adiabatic approximation in ADK theory, $\frac{\langle \Psi_m | \frac{\partial}{\partial t} \hat{H} | \Psi_n \rangle}{\varepsilon_m - \varepsilon_n} \ll 1$ [See Appendix D]. When the laser frequency is much smaller than the characteristic frequency of electron, the electron will have sufficient time to follow the change of the laser field. Eq. (2.48) shows that at the saddle point t_s, $\cos(\omega t_s)$ is approximately equals to one. This correspond to the electric field maximum, which implies the tunneling ionization will mostly happened near the peak of the electric field.

2.5 The origin of the ATI peaks

Assume the laser pulse is infinitely long and given by

$$\vec{E}(t) = \vec{E}_0 \cos \omega_L t \quad \text{and} \quad \vec{A}(t) = -\frac{\vec{E}_0}{\omega_L} \sin \omega_L t. \tag{2.55}$$

The classical action given by eq. (2.34) can be integrated exactly:

$$S(t) = -\left(\frac{k^2}{2} + I_p + U_p\right) t + \frac{\vec{k} \cdot \vec{E}(t)}{\omega_L^2} - \frac{U_p}{\omega_L} \sin 2\omega_L t \tag{2.56}$$

Substituting this equation into eq. (2.35), we obtain

$$(S-1)_{fi}^{SFA} = \left[-\tilde{\phi}_g(\vec{k} + \vec{A}) e^{iS(t)}\right]_{-\infty}^{+\infty} + \int_{-\infty}^{+\infty} dt\ \Omega(t) e^{i\left(\frac{k^2}{2} + I_p + U_p\right)t} \tag{2.57}$$

where

$$\Omega(t) = S'(t) \tilde{\phi}_g e^{iS(t) - i\left(\frac{k^2}{2} + I_p + U_p\right)t}$$

has a period of $T = \frac{2\pi}{\omega_L}$. Hence we can expand $\Omega(t)$ in a Fourier series expansion

$$\Omega(t) = \sum_n L_n(\vec{k}) e^{-in\omega_L t} \tag{2.58}$$

Using the above relation and evaluating the time integral in eq. (2.57), we obtain [39]

$$(S-1)_{fi}^{SFA} = 2\pi i \sum_n \delta\left(\frac{k^2}{2} + I_p + U_p - n\omega_L\right) L_n(\vec{k}) \tag{2.59}$$

The delta function enforces the conservation of energy, and the photoelectron spectrum will show a series of peaks. All the peaks are separated by exactly one photon energy. We can interpret these peaks as arising from the electron absorbing more photons than necessary to conquer the potential barrier and then entering the continuum with excess energy. This is a generalization of Einstein's photon electron energy formula for the photoelectric effect.

Chapter 3

The 1-D model

In numerical simulation of intense field ionization, the amount of space-time grids involved in the ionization process is huge. The number of atomic or molecular states involved in the ionization process is also huge. As a result, *ab initio* simulation is extremely computational intensive. So we simplify the calculation by reducing the dimensionality of the system [19, 35, 13]. In the case of linearly polarized laser focusing on a hydrogen atom, excitation is most effective along the direction of the laser polarization, and the one dimensional model should describe the physics reasonably well. Most importantly, using this simple model we will be able to test some of the fundamental assumptions employed in theories proposed in the past few decades.

In this Chapter we will consider a one-dimensional model atom and a molecular ion with the nuclei being clamped. This is the first step towards understanding the intense laser pulse interaction with matter. Before we give a mathematical form of the model we should first of all have some ideas about the range of physical parameters that will be of interest in the calculation. The laser intensity will be around 10^{14} W/cm^2, the wavelength is about 900 nm and the pulse length is around 20 fs. The ionization potential for our one-dimensional ground state atom is 18 eV (about 0.7 atomic unit). The wave length is about 900 times larger than the size of the model atom. The kinetic energy of the electron after laser pulse interaction can reach 80 eV so that the electron wave function span will be approximately within 100 nm. The root mean square deviation of the wave function will be approximately 10 nm; thus most of the electron probability is concentrated within

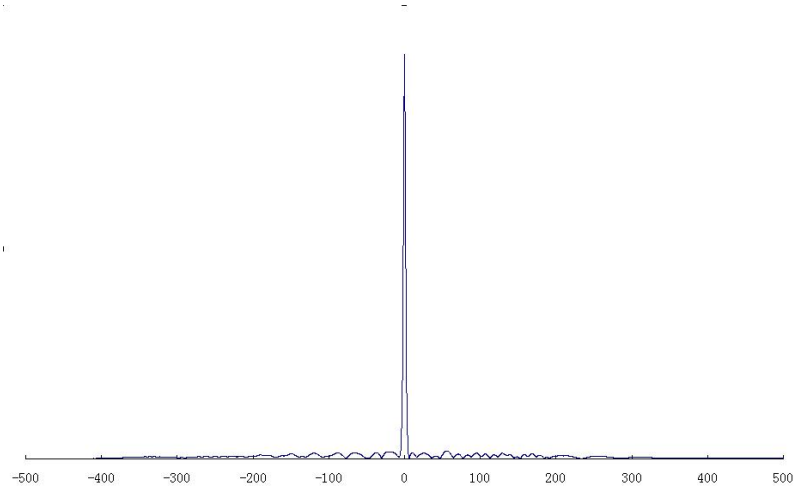

Figure 3.1: Electron wave function after 4-cycle laser interaction. The horizontal axis is is the space coordinate in atomic unit.

a narrow region close to the core (See Figure 3.1).

3.1 Time-dependent Schrödinger equation

The time evolution of the electron in one-dimension is described by the time-dependent Schrödinger equation

$$i\frac{\partial}{\partial t}\Psi(x,t) = \hat{H}(x,t)\Psi(x,t) \tag{3.1}$$

where the total Hamiltonian is

$$\hat{H}(x,t) = \hat{T} + \hat{V}_a(x) + \hat{V}_L(x,t), \tag{3.2}$$

and the kinetic energy operator is

$$\hat{T} = -\frac{1}{2}\frac{\partial^2}{\partial x^2}. \tag{3.3}$$

The binding potential $\hat{V}_a(x)$ is a function of coordinate only. We can study several different forms of the binding potential so that the correlations with the photo-electron

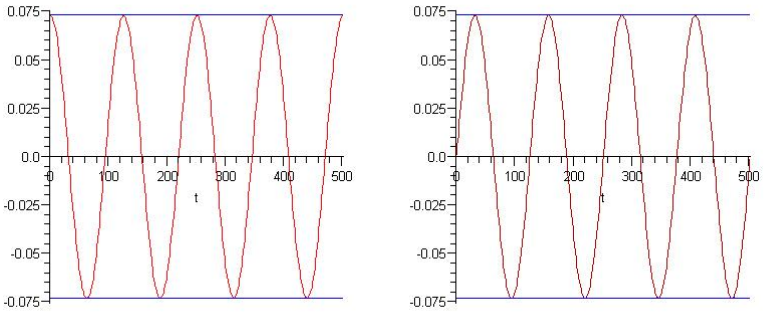

Figure 3.2: Laser pulses with the square envelope. $E_0 = 0.075$ and $\varphi = \frac{\pi}{2}$ (left panel) $\varphi = 0$ (right panel).

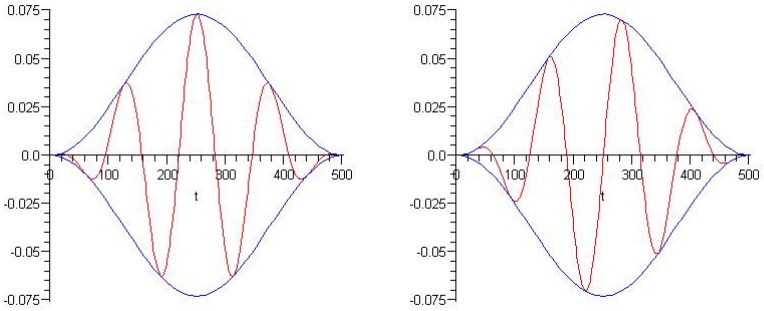

Figure 3.3: Laser pulses with the sine-square envelope. $E_0 = 0.075$ and $\varphi = \frac{\pi}{2}$ (left panel) $\varphi = 0$ (right panel).

spectrum may be revealed. We will specifically work in the length gauge so that the interaction Hamiltonian takes the form

$$\hat{V}_L(x,t) = xE(t). \tag{3.4}$$

where $E(t)$ is the electric field of the laser pulse represented by

$$E(t) = E_0 f(t)\sin(\omega_L t + \varphi). \tag{3.5}$$

$f(t)$ is the envelope function. We use two different envelope functions in our study. The first one is a square pulse envelope (see Figure 3.2):

$$f(t) = \begin{cases} 1, & \text{if } 0 \le t \le T_p \\ 0, & \text{otherwise} \end{cases}$$

and the second one is a sine-square pulse envelope (see Figure 3.3):

$$f(t) = \begin{cases} \sin^2(\frac{\omega_p}{2}t), & \text{if } 0 \le t \le T_p \\ 0, & \text{otherwise.} \end{cases}$$

φ in eq. (3.5) is known as the carrier envelope phase (CEP). This CEP is an important parameter for the dynamics of ultrashort laser pulse ionization of atom. We study the time evolution of the wave packets by the split operator method using fast Fourier transform where we express the wave function in terms of the evolution operator as

$$\Psi(x,t) = \hat{U}(0,t)\Psi(x,0). \tag{3.6}$$

We discretize the time variable and propagate the wave function according to

$$\Psi(x,t+\Delta t) \approx \exp\left[-i\hat{T}\Delta t\right]\exp\left[-i\left(\hat{V}_a(x) + \hat{V}_L(x,t)\right)\Delta t\right]\ \Psi(x,t) \tag{3.7}$$

The time evolution becomes computable after the splitting of the non-commuting potential and kinetic energy operators. We can perform the potential propagation in coordinate representation and the kinetic energy propagation in momentum representation, the conversion between these two representations being carried out by the fast Fourier transform. After the end of the wave function propagation, we project it onto a positive energy continuum state of the atom or molecule:

$$\left[\hat{T} + \hat{V}_a(x)\right]\phi_\epsilon(x) = \epsilon\phi_\epsilon(x), \quad \epsilon > 0 \tag{3.8}$$

and the photoelectron spectrum is obtained from

$$P(\epsilon) = |\langle\phi_\epsilon(x)|\Psi(x,t_f)\rangle|^2 \tag{3.9}$$

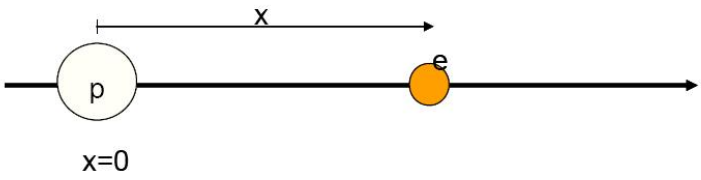

Figure 3.4: A schematic diagram for the one dimensional atom. The nucleus is clamped at the origin; therefore, we only have one degree of freedom.

3.2 One-Dimension model atom and photoelectron spectrum

The intense laser pulse ionization of an one-dimensional model atom is first studied by Eberly and Javanainen [11]. A schematic diagram of the model is shown in Figure 3.4. The model atom has a potential given by:

$$\hat{V}_a(x) = -\frac{1}{\sqrt{(1+x^2)}}. \tag{3.10}$$

This soft-core potential has a Coulomb tail and it is analytic at the origin. According to [19] it is realistic in the sense that it has a Rydberg series structure and it preserves parity. By using standard finite difference method [34] we solve the eigenvalue problem of eq. (3.8). The first 8192 states of the atomic system are obtained. They are non-degenerate and almost complete in the sense that the probability for the photoelectron to obtain energy greater than 9 a.u. is negligible. We plot the energy of the first 150 states in Figure 3.5. The ground state energy is -0.67 a.u. The first 57 states are bounded states and the rest are positive energy scattering states which we used in eq.(3.9) to obtain the photoelectron spectrum.

Before going to detailed analysis, let us take a look at the general features of the photo-electron spectrum (PES). A typical ATI spectrum is shown in Figure 3.7. The horizontal axis labels the atomic scattering states by their energy eigenvalues. When an electron is kicked into the continuum it will have some probability to occupy one of these scattering states. In Figure 3.7 the spectrum is cut off at the photoelectron energy

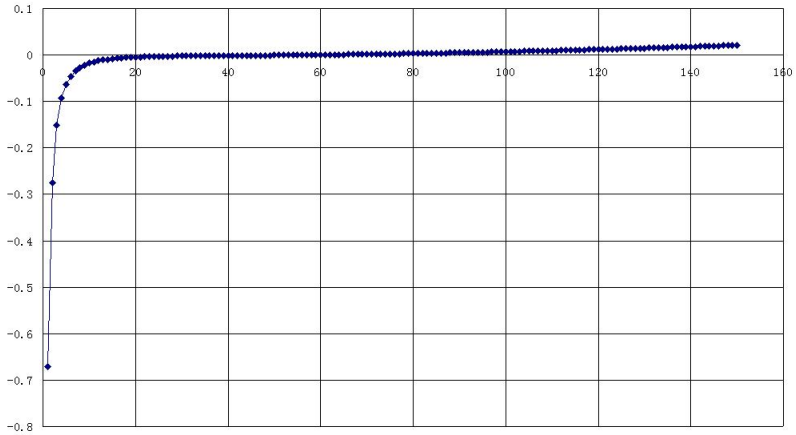

Figure 3.5: We plot the first 150 eigenstates of the atomic potential (3.10). The bound states have discrete energy levels. The continuous states have positive energy levels and are sufficiently close to each other so that they can be used as bases for photoelectron spectra.

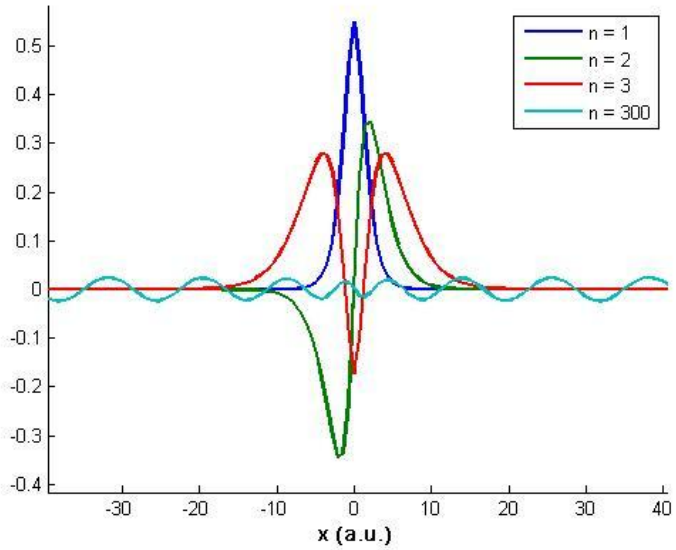

Figure 3.6: Eigenfunctions for the three lowest bound states and a typical continuum state (n=300). As we can see the parity alternates as n increases.

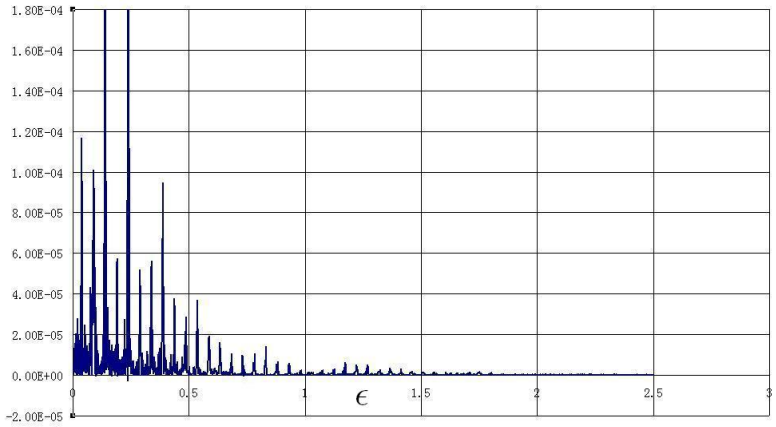

Figure 3.7: A 4-cycle laser with square pulse envelope interact with 1-D atom. The frequency is 0.05 a.u. and the laser intensity is 0.073 a.u. ϵ is the eigenvalue for the continuous states i.e. the energy.

of 1.7 a.u. which can be understood as the maximum energy an electron can acquire from this strong field ionization. Intuitively, this cutoff will depend on field intensity, laser frequency and the ionization potential of the atom. There is a semi-classical model which provides an explanation to this spectrum [31]. The idea is that at some time after the laser is turned on, the electron tunnels out the potential barrier and appears in the continuum with approximately zero kinetic energy. The freed electron then is driven by the intense laser field. Depends on the moment when electron appears in the continuum we may see some electrons be driven away from the nuclear core and never come back. These electrons are called direct electrons which give rise to the direct electron term of the transition amplitude. Calculation shows that they will have maximum kinetic energy $2U_p$ where U_p is the pondermotive energy $U_p = \frac{E_0^2}{4\omega^2}$. Another significant feature of the electron spectrum is its comb-like structure. The peaks are separated by exactly one photon energy. This indicates that the electron can absorb more photons than the minimum required to conquer the potential barrier. Actually this comb structure is due to an interference of the transition amplitudes at different moment of release of photoelectron.

3.3 Dependence of ionization on physical parameters

The problems we are interested in strong field physics can be briefly categorized as three types. The first type is to have a well known and controllable laser pulse focus on an atomic or molecular system so that through detecting the light emission or the kinetic energies of the photoelectron and/or residue ions, we can obtain information of the system itself. The other type of question is to use atoms whose properties are known as probes of the laser pulses so that we can obtain information of the pulse characteristics including pulse shape, intensity, frequency and carrier-envelope phase. The last type of question is to use a well controlled laser pulse to induce electron dynamics of a system so as to control the molecular dynamics of the parent ions. In order to realize the above goals we should understand how the physical parameters affect the photoelectron spectrum.

3.3.1 Dependence on pulse length and pulse shape

From the Fourier transform relations, the shorter the pulse length the broader the laser spectrum will be. As we can see from Figure 3.8 and Figure 3.9, the peaks of a four cycle laser ionization spectrum are broader than those of eight cycle laser ionization spectrum for the same laser intensity. The outline of the spectrum changes very little but its magnitude increases for the longer pulse as expected. It is a result of accumulation of transition amplitude from different cycles.

The photoelectron spectra for the square envelope pulses have sharper lines compared with those of sine-square envelope pulses. We also observe that as we increase pulse length, the higher energy region of photoelectron spectrum is suppressed relative to the lower energy region as shown in Figure 3.10 with a comparison of Figure 3.11. This is due to the fact that as we increase the pulse length, the electron wave function will be spread out more instead of mostly concentrated in the core region (Figure 3.1), reducing the probability of electron re-scattering with the core. Thus the spectrum in the high energy region is suppressed.

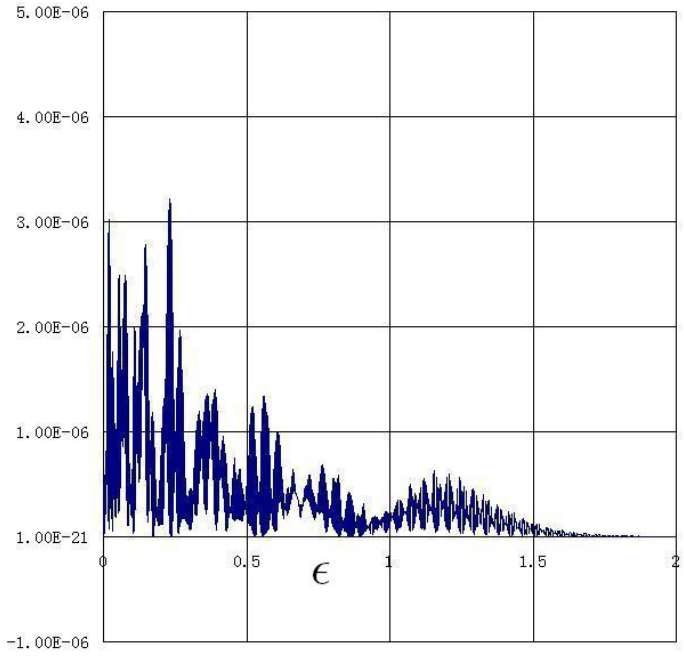

Figure 3.8: Spectrum for a 4 cycle sine-square envelope laser pulse interacting with a 1-D atom. $E_0 = 0.073$ a.u, $\omega_L = 0.05$ a.u. and $\varphi = \frac{\pi}{2}$.

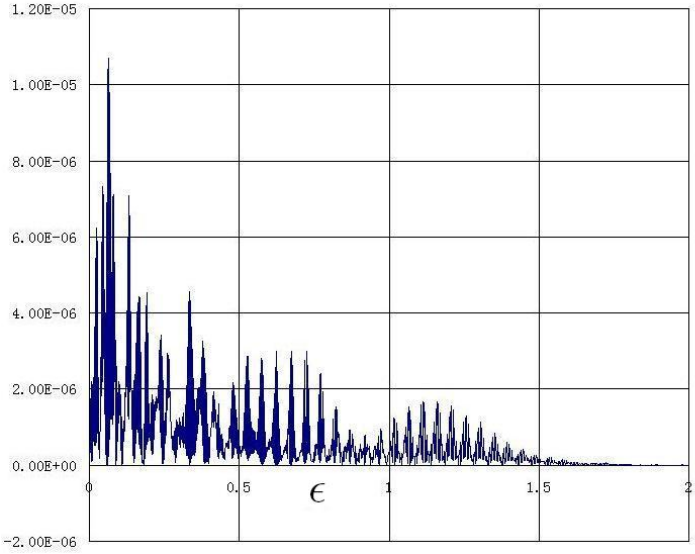

Figure 3.9: Spectrum for an 8 cycle sine-square envelope laser pulse interacting with a 1-D atom. $E_0 = 0.073$ a.u, $\omega_L = 0.05$ a.u. and $\varphi = \frac{\pi}{2}$.

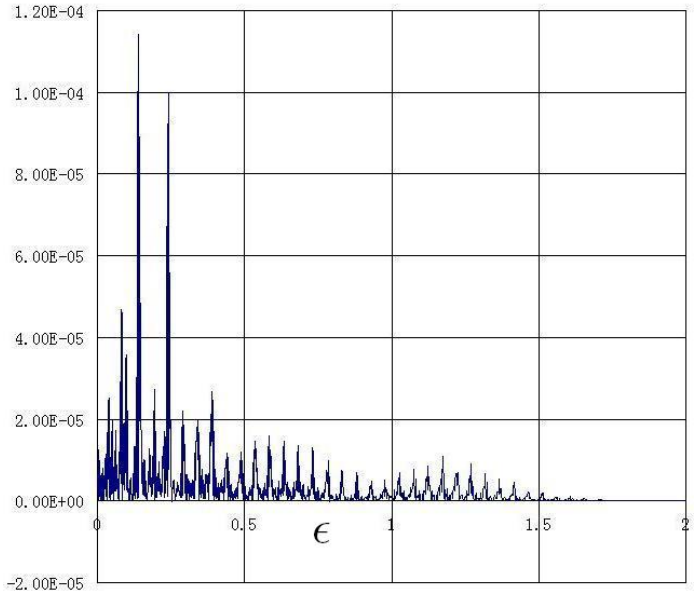

Figure 3.10: Spectrum for a 4 cycle square envelope laser pulse interacting with a 1-D atom. $E_0 = 0.073$ a.u, $\omega_L = 0.05$ a.u. and $\varphi = \frac{\pi}{2}$.

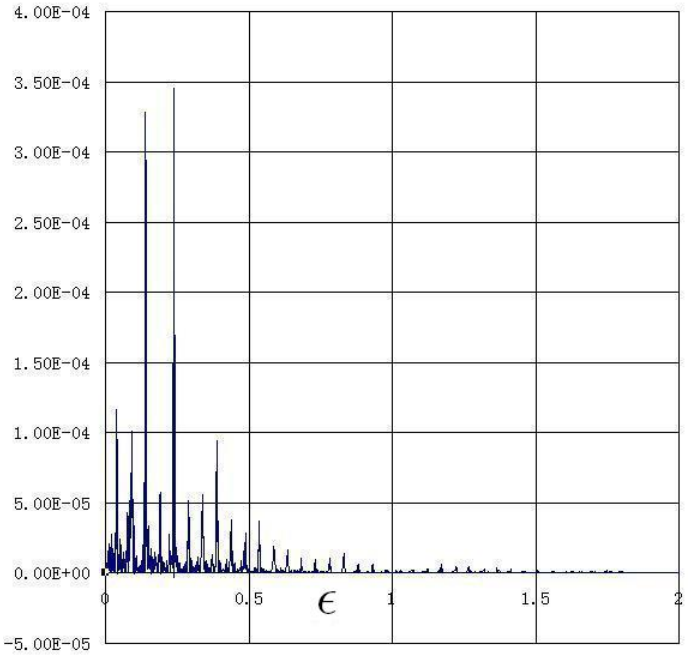

Figure 3.11: Spectrum for an 8 cycle square envelope laser pulse interacting with a 1-D atom. $E_0 = 0.073$ a.u, $\omega_L = 0.05$ a.u. and $\varphi = \frac{\pi}{2}$.

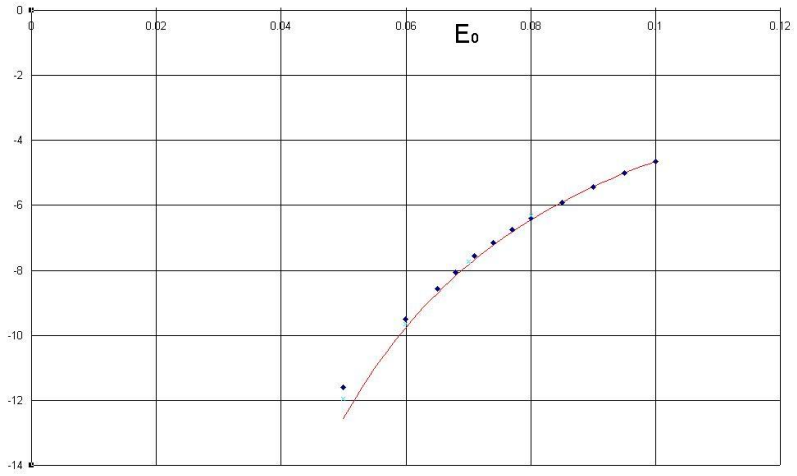

Figure 3.12: The total ionization probability versus field strength E_0 plotted in semi-log scale (vertical axis is in log scale). The blue dots are from numerical calculation for a sine-square envelope laser pulse. The red line is calculated by an ADK-type formula. We choose the pre-exponential factor to be $E_0^{-7/2}$.

3.3.2 Dependence on intensity

As we increase the laser intensity the total ionization rate will also increase. In the tunneling region the ionization rate is given by eq.(2.54). However for the 1-D model atom the pre-exponential factor may be different from the 3-D hydrogen atom. We plot the total ionization rate from TDSE calculation and fit the data to obtain a pre-exponential factor (see Figure 3.12). The matching between TDSE and ADK-type calculation implies the tunneling behavior of the system. As we further decrease the laser intensity, the Keldysh parameter becomes greater than one so that multiphoton ionization dominates, and the ADK formula will not be applicable.

The semi-log plot of the photoelectron spectrum will show a clear cutoff at $2U_p$ [40]. This cutoff is well explained by a semi-classical model, which assumes that the electron tunnels out at the maximum of electric field with zero kinetic energy. Subsequently it is driven by the laser field as a free electron [9]. Since U_p is proportional to the laser intensity we observe that the cutoff shifts to the higher energy region as we increase E_0 (see Figure 3.13 - Figure 3.15).

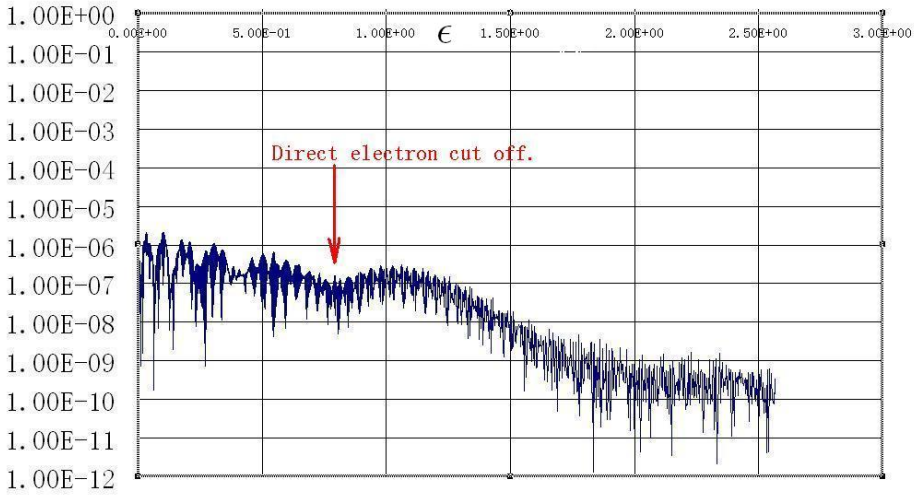

Figure 3.13: A semi-log plot of PES of a 4-cycle sine-square envelope laser pulse ionization of the atom. $E_0 = 0.068$ a.u. $\varphi = \frac{\pi}{2}$ and $\omega_L = 0.05$ a.u.

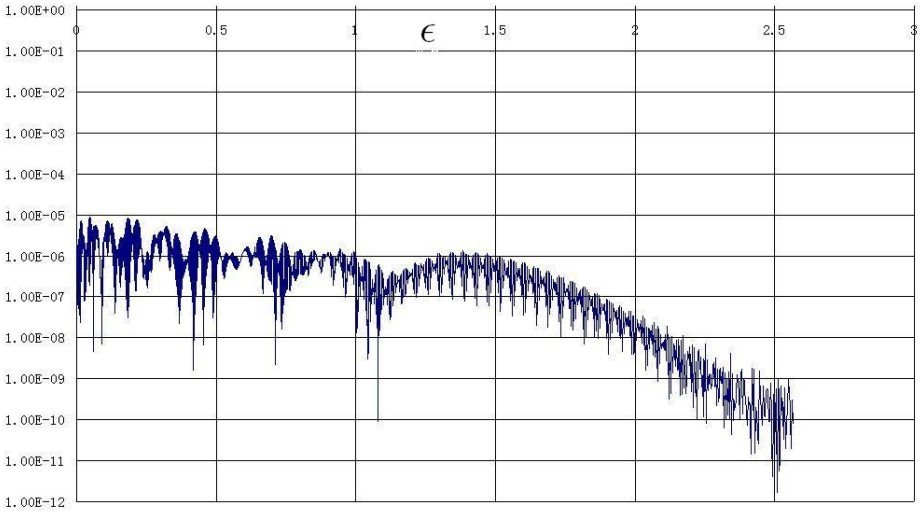

Figure 3.14: A semi-log plot of PES of a 4-cycle sine-square envelope laser pulse ionization of the atom. $E_0 = 0.08$ a.u. $\varphi = \frac{\pi}{2}$ and $\omega_L = 0.05$ a.u.

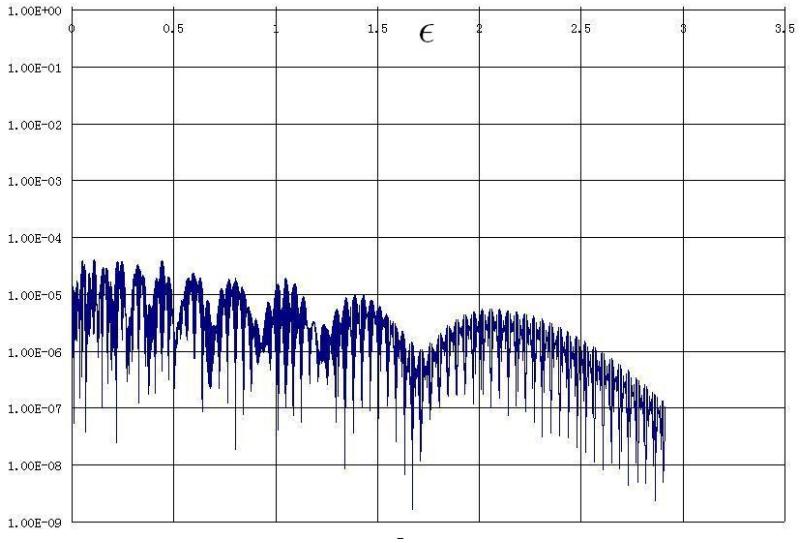

Figure 3.15: A semi-log plot of PES of a 4-cycle sine-square envelope laser pulse ionization of the atom. $E_0 = 0.1$ a.u. $\varphi = \frac{\pi}{2}$ and $\omega_L = 0.05$ a.u.

3.3.3 Dependence on CEP

We compared the spectra for different CEPs in Figure 3.16-3.19. We can see that from Figure 3.16-3.17 for a sine-square envelope pulse, the high energy part of the spectrum for the $\varphi = \frac{\pi}{2}$ case is enhanced compare to the $\varphi = 0$ case. This enhancement is stronger at the higher intensity, which means that at high intensity the spectrum becomes more sensitive to CEP.

In the case of square-envelope pulse we find that the spectrum is extremely sensitive

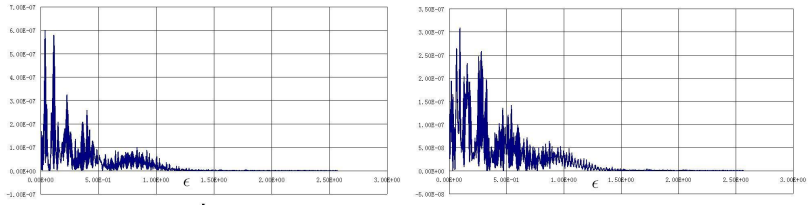

Figure 3.16: The PES for a 4-cycle sine-square envelope laser pulse ionization of the atom. $E_0 = 0.06$ a.u. $\varphi = \frac{\pi}{2}$ (left panel) and $\varphi = 0$ (right panel).

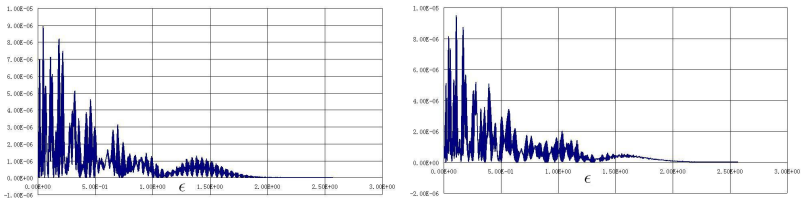

Figure 3.17: The PES for a 4-cycle sine-square envelope laser pulse ionization of the atom. $E_0 = 0.08$ a.u. $\varphi = \frac{\pi}{2}$ (left panel) and $\varphi = 0$ (right panel).

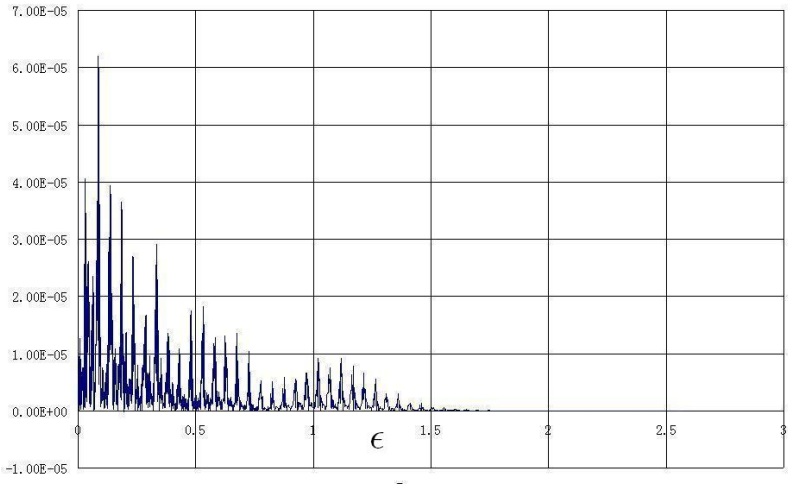

Figure 3.18: The PES for a 4-cycle square envelope laser pulse ionization of the atom. $E_0 = 0.07$ a.u. and $\varphi = \frac{\pi}{2}$.

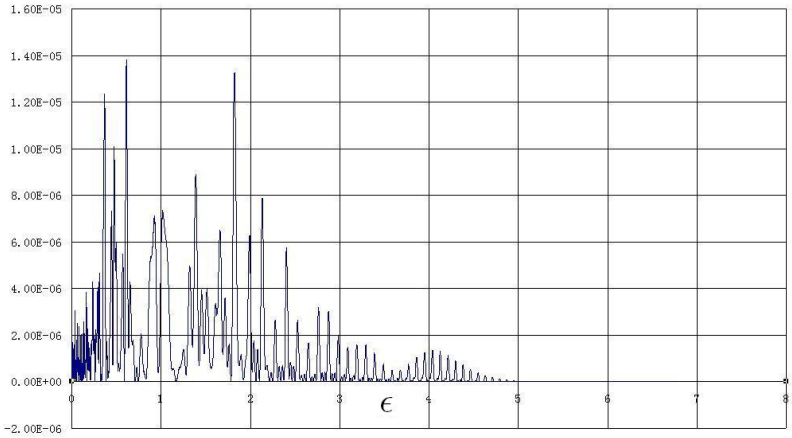

Figure 3.19: The PES for a 4-cycle square envelope laser pulse ionization of the atom. $E_0 = 0.07$ a.u. and $\varphi = 0$.

to CEP. As we can see in Figure 3.18, for $\varphi = \frac{\pi}{2}$, the photoelectrons mostly appear in the low energy region with regular ATI structure. When we switch to $\varphi = 0$ as shown in Figure 3.19, the photoelectron spectrum becomes irregular and extends to the high energy region. The higher energy peaks are not separated by a single photon energy.

From the above observation we conclude that in order to make the spectrum sensitive to the CEP, two conditions should be met. First of all the laser intensity must be high so that ionization is in the tunneling region. Secondly the pulse should be very short so that the spectrum is an accumulation of photoelectrons for only a few cycles. It also appears that the square envelope is more effective than a sine-square envelope pulse.

3.4 Comparison between SFA and TDSE Calculation

The transition amplitude introduced by Keldysh in 1965 [20] corresponds to the direct electron term in the intense field many-body S-matrix theory [5]. It is possible to give a physical interpretation to this term. Initially the electron is at its ground state. At some time t' it is kicked into continuum by the laser field, and from then on, it is driven only by the laser field and assumed not to feel the core potential again (see Figure 1.2). This is an approximation called the strong field approximation (SFA). The gauge invariance is destroyed under the SFA. Even though several papers [21, 22, 4] have been done to resolve the gauge dependence problem, there is still no rule to tell us what gauge we should choose. The length gauge is generally used in the case of atoms and diatomic molecules; however, there is still no satisfactory explanation why the length gauge works better [4].

To test the validity of SFA, we will make a comparison of SFA calculations in the length gauge with TDSE calculations of the one dimensional model. We calculate the direct electron term of eq. (2.30)

$$(S-1)_{fi} = -i \int_{t_i}^{t_f} dt' \langle \psi_f(t') | \hat{V}_L(t') | \phi_i(t') \rangle$$

by evaluating the integral numerically. The hope is to find out what are the conditions for SFA to be valid. First of all we will study the case of half cycle laser pulse.

3.4.1 Half cycle laser pulse

Electron dynamics in a half cycle laser pulse is much simpler than many cycle pulses because there is no accumulation of transition amplitude from different cycles. The photoelectron spectra for the CEP $\varphi = 0$ and $\varphi = \frac{\pi}{2}$ obtained from TDSE calculation are plotted in Figure 3.21 and Figure 3.24 while those obtained from SFA are given in Figures 3.22, 3.23 and Figure 3.24. In the case of $\varphi = 0$, the SFA calculation tends to underestimate the photo-electron energies. As we can see in Figures 3.21 and 3.22 the TDSE calculation predicts a spectrum extending to about 6 a.u, but SFA spectrum only extends to 3.5 a.u. However, the SFA calculation is gauge dependent; we add a constant

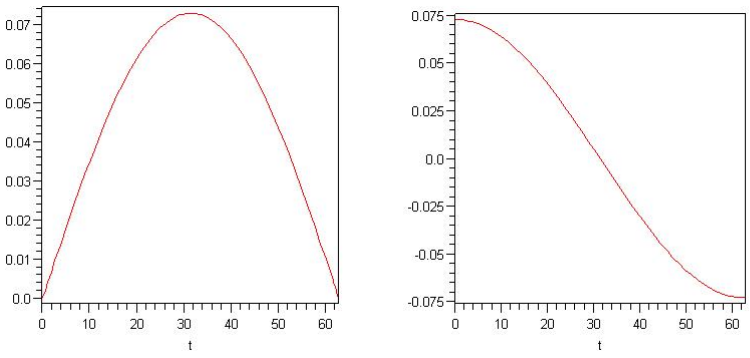

Figure 3.20: Half cycle laser pulses with $E_0 = 0.073$ a.u. The CEPs are $\varphi = 0$ and $\varphi = \frac{\pi}{2}$ respectively.

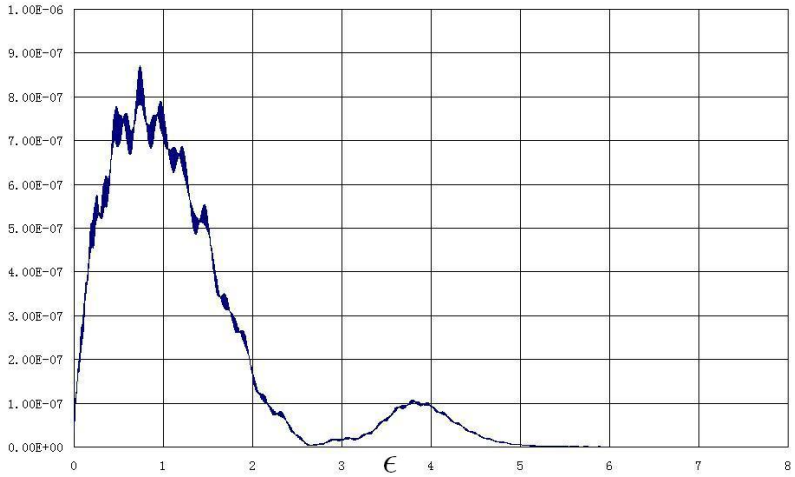

Figure 3.21: The photo-electron spectrum for half cycle laser pulse ionization of atom. The CEP is $\varphi = 0$ and $E_0 = 0.073$ a.u. The frequency is $\omega_L = 0.05$ a.u.

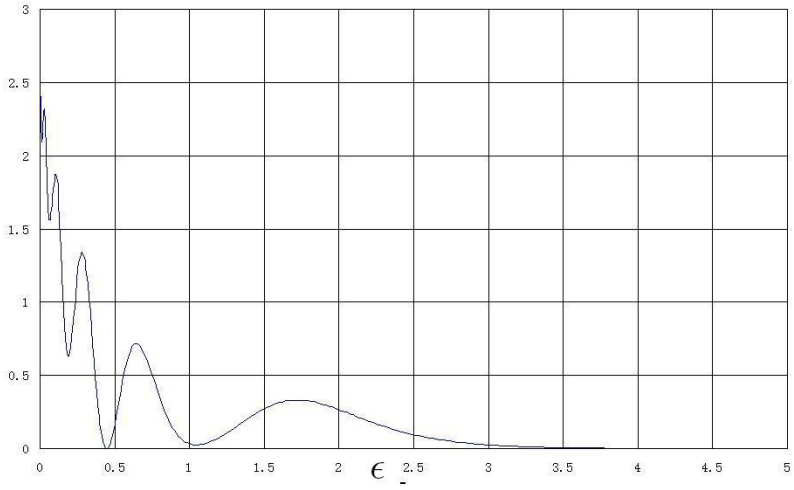

Figure 3.22: SFA calculation of PES of the atom ionized by a half cycle laser pulse with $E_0 = 0.073$ a.u. and $\varphi = 0$.

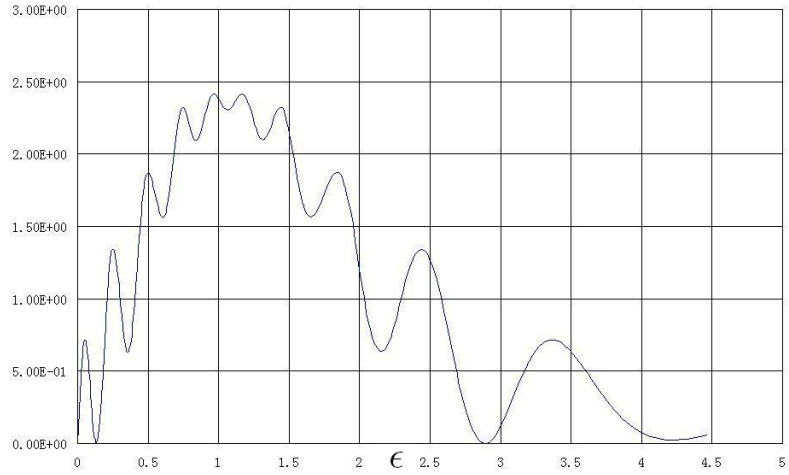

Figure 3.23: SFA calculation of PES of the atom ionized by a half cycle laser pulse with $E_0 = 0.073$ a.u. $\varphi = 0$. We add a constant vector in the vector potential through the gauge transformation eq. 2.4. This new spectrum is the spectrum 3.22 shifted to the positive direction.

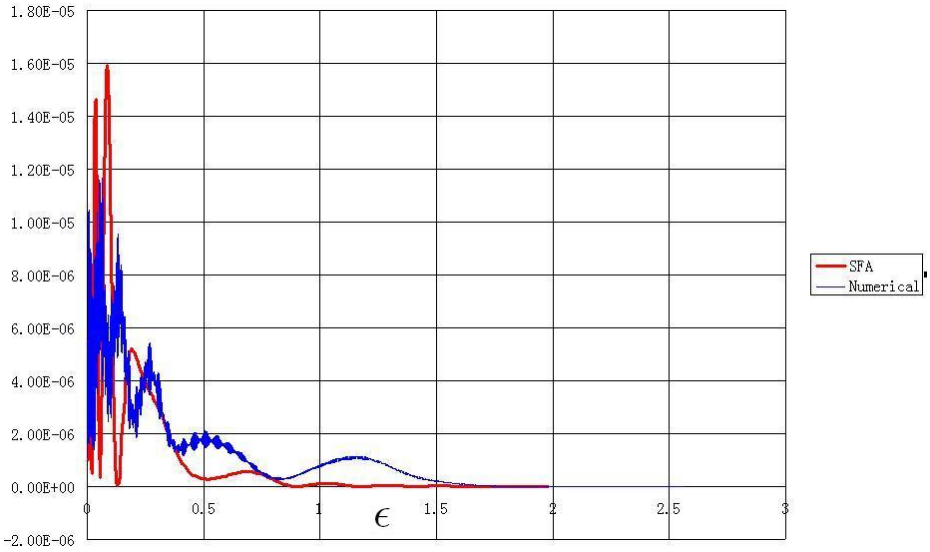

Figure 3.24: The comparison between PES from SFA calculation and TDSE calculation. It is a half cycle laser pulse with $E_0 = 0.073$ a.u. $\varphi = \frac{\pi}{2}$.

vector to the vector potential in Volkov state of eq. (C.5). This constant vector potential will not change the electric field but it will shift the photoelectron spectrum to higher energies. As shown in Figure 3.23 we can choose this constant vector potential properly to match the SFA and TDSE calculations. In general we found the condition $A(0) = 0$ should be used.

When the laser CEP $\varphi = \frac{\pi}{2}$, the SFA and TDSE spectra will roughly match as shown in Figure 3.24. Since the model potential is a long range potential, and within the half cycle duration the electron density is still concentrated in the region close to core, we do not expect SFA to be a very good approximation. The high energy portion of the the numerical spectrum has been greatly suppressed in the case of $\varphi = \frac{\pi}{2}$. Because most photoelectrons will be ionized at the peak of the electric pulse with certain kinetic energy E_k and after ionization the propagation is due to the vector potential A. The electric field ends at maximum meaning the vector potential ends at zero. Therefore, the mechanical momentum of electrons reach minimum at the end of the pulse. Hence high energy photoelectrons are not generated.

3.4.2 A four-cycle laser pulse

For a square-envelope four cycle laser pulse the situation is very similar to the half cycle pulse case. The spectrum is very sensitive to the carrier envelope phase. Here we will only compare the SFA calculation with TDSE calculation for the pulse that has CEP $\varphi = \frac{\pi}{2}$. As we can see in Figure 3.25 the SFA calculation underestimates the high energy region of the photo-electron spectrum. When we increase the laser intensity, the spectrum extends to higher energy region; however, the SFA still underestimates the high energy region of the spectrum. This is because the high energy region of the spectrum is due to the Coulomb effects during ionization. SFA calculations neglect the Coulomb effects. More explicitly, the SFA calculation does not include the polarization and re-scattering effects.

In the case of sine-square envelope pulse the SFA calculation has two major deviations from the TDSE calculation. First of all, the SFA calculation underestimates the high energy region of the spectra. Secondly, the low energy regions of the spectra do not show regular structures (see Figure 3.26 and Figure 3.27). As in the case of the square-envelope pulse, we only include the direct electron term in the SFA calculation; however, TDSE calculation includes both direct and re-scattering electrons. The re-scattering electrons mainly contribute to the high energy region in the spectra so that SFA tends to underestimate the high energy region. In addition, the core potential is a long range potential so the strong field approximation is not expected to be good even in the tunneling region for such a short pulse. When the laser pulse is very short, the electron density is mostly concentrated at the region close to core during the interaction period, especially for the low energy electrons. If we further increase the laser intensity, better agreement is found in the intermediate energy region. (See Figure 3.28 and Figure 3.29). For a short range potential we can get very good agreement in both the low and intermediate energy regions [3].

3.4.3 Short range potential

The tail of long range atomic potential is the main reason for the failure of SFA spectrum in the high energy region. In order to demonstrate this idea we modify the atomic

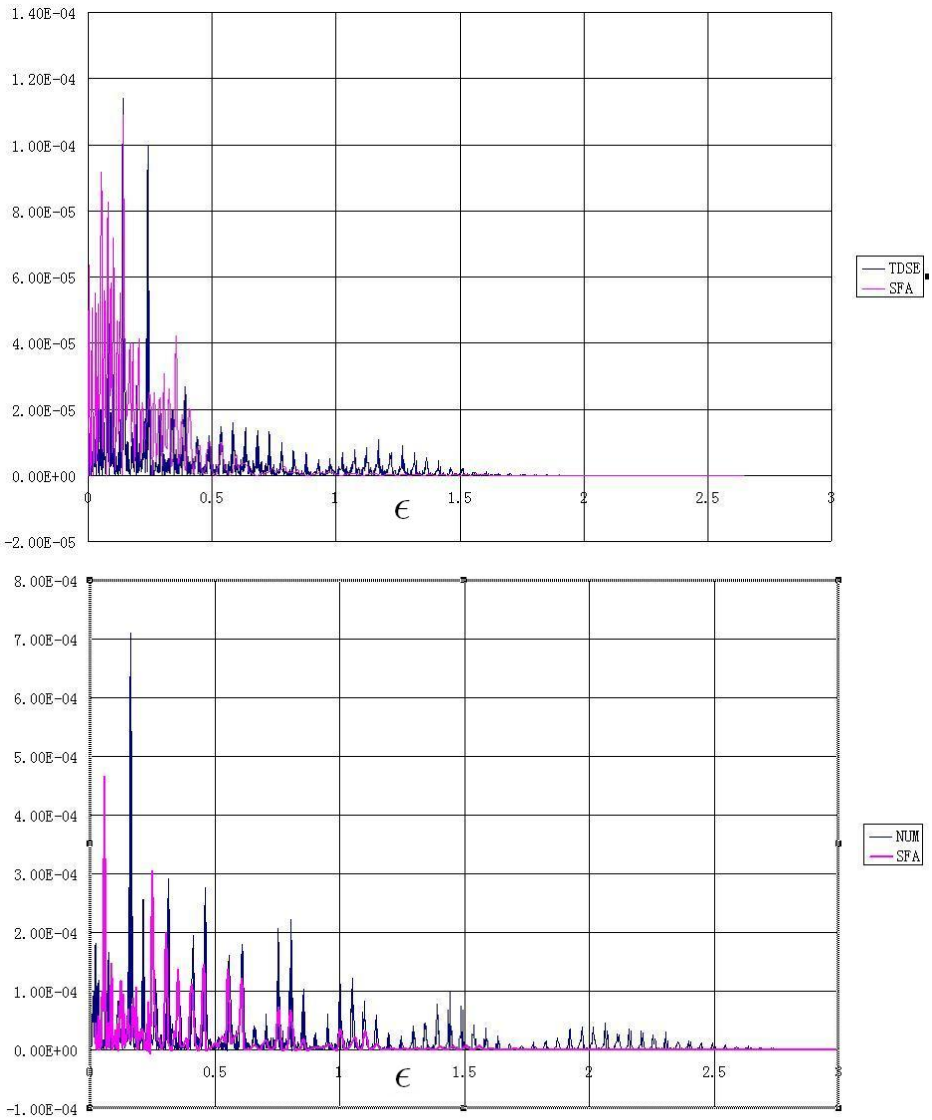

Figure 3.25: The comparisons between SFA and TDSE calculation of PES for a 4-cycle square envelope laser pulse with $E_0 = 0.073$ a.u. (above diagram) and $E_0 = 0.1$ a.u. (below diagram). $\varphi = \frac{\pi}{2}$.

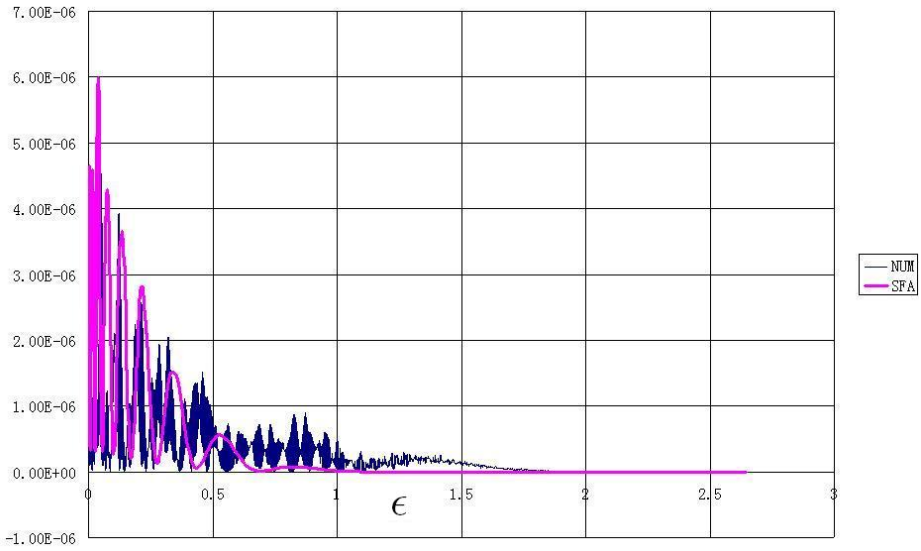

Figure 3.26: The comparison between SFA and TDSE calculation of PES for a 4-cycle sine-square envelope laser pulse with $E_0 = 0.073$ a.u. $\varphi = 0$.

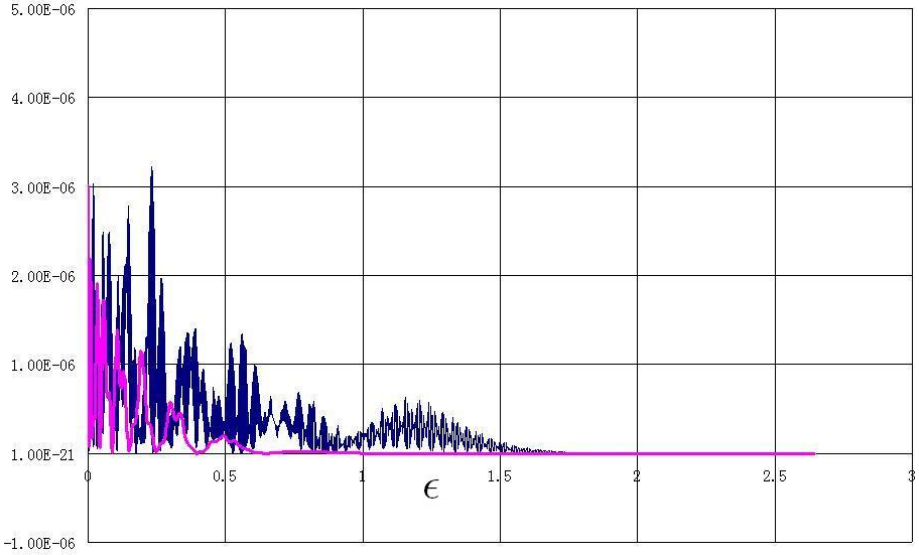

Figure 3.27: The comparison between SFA and TDSE calculation of PES for a 4-cycle sine-square envelope laser pulse with $E_0 = 0.073$ a.u. $\varphi = \frac{\pi}{2}$.

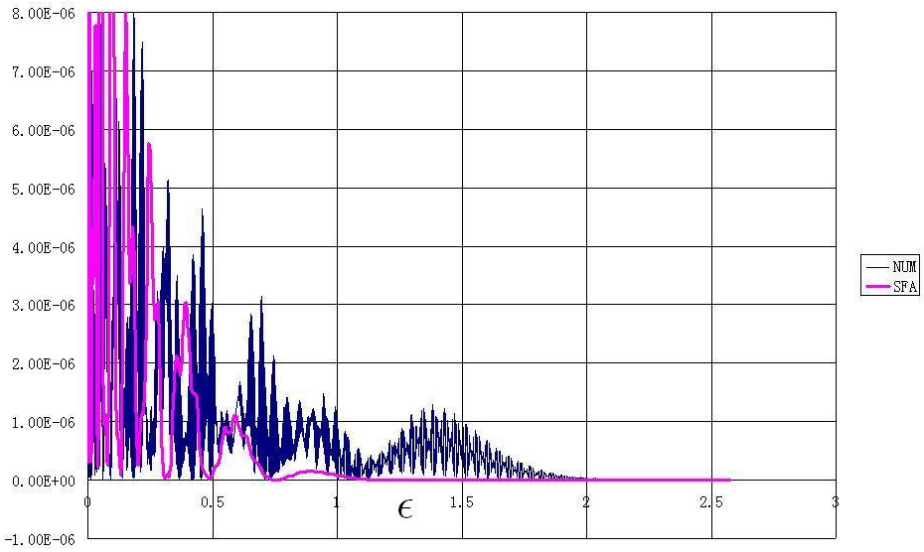

Figure 3.28: The comparison between SFA and TDSE calculation of PES for a 4-cycle sine-square envelope laser pulse with $E_0 = 0.08$ a.u. $\varphi = \frac{\pi}{2}$.

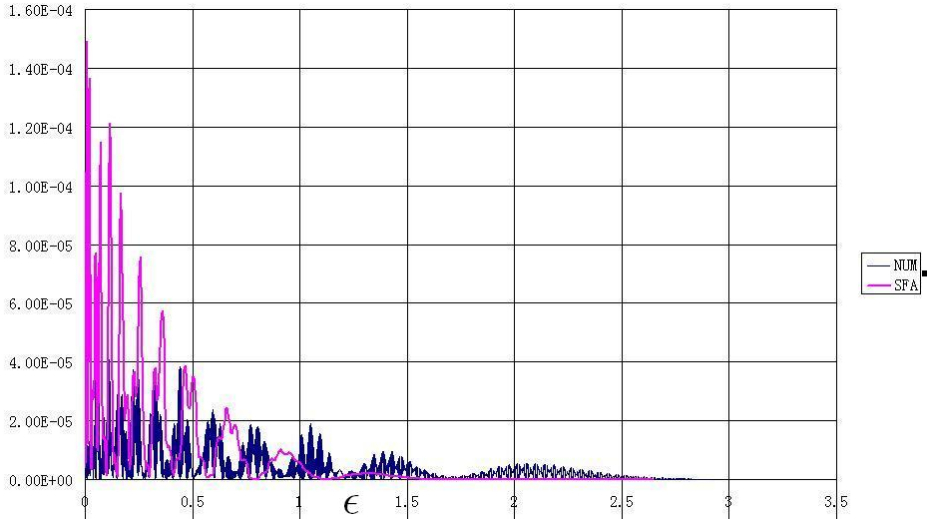

Figure 3.29: The comparison between SFA and TDSE calculation of PES for a 4-cycle sine-square envelope laser pulse with $E_0 = 0.1$ a.u. $\varphi = \frac{\pi}{2}$.

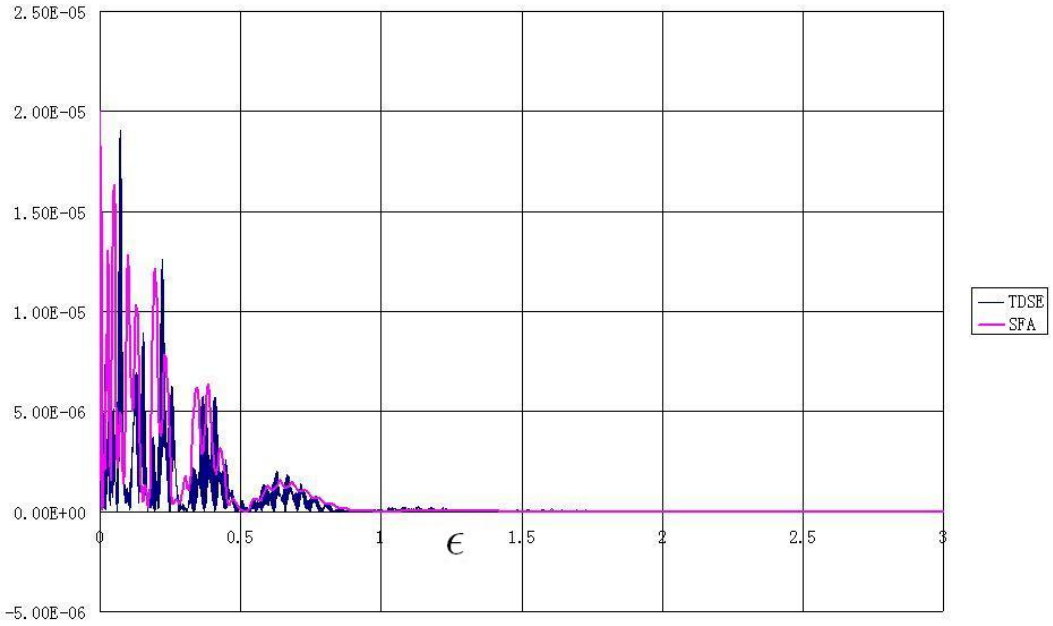

Figure 3.30: The comparison between SFA and TDSE calculation of PES for a 4-cycle sine-square envelope laser pulse with $E_0 = 0.073$ a.u. $\varphi = \frac{\pi}{2}$. The Coulomb tail of the atomic potential is screened by an exponential factor as described in the text.

potential as following:

$$\frac{1}{\sqrt{1+x^2}} \longrightarrow \frac{\exp(-\alpha x^2)}{\sqrt{1+x^2}}$$

The constant α can be chosen as 0 or 1, corresponding to a long range or short range potential, respectively. The comparison between the TDSE and the SFA spectra is shown in Figure 3.30. As we switch from a long range potential to a short range potential, the high energy region of photo-electron spectrum obtained from the TDSE is significantly suppressed. This implies that the electron bounded by a short range potential has less capability of gaining energy than the electron bounded by long range potential. It happens because the polarizability of the two systems are different. The atom with a long range potential will have a larger polarizability. Thus electron will be pulled away from the core before being ionized, and it will gain large amount of energy. However, for the electron bounded by a short range potential, the polarizability is small. Thus the electron cloud will be distorted only a little before ionization, and only small amount of energy is gained, giving rise to the supression of the high energy region of the spectrum. Later, we will see that the same reason applies to the molecular ion case.

3.5 The probability current

We also look at the electron probability current during the interaction with the laser field. Within four cycles the electron will not have time to escape from the region of calculation. Therefore the total probability in the region should be conserved. We divided the region into three parts as shown in Figure 3.31. Initially the electron is in the ground state so that most population is in the core region. After the laser field is turned on, the population in all three regions will change in time. Because of the conservation of probability, we have

$$-\frac{\partial}{\partial t}\rho_1 = j_{12} \tag{3.11}$$

where ρ_1 is the population in region 1 and j_{12} is the probability current flow through the boundary 12. Similarly, the rate of change of population in core region is given by

$$-\frac{\partial}{\partial t}\rho_{core} = j_{23} - j_{12} \tag{3.12}$$

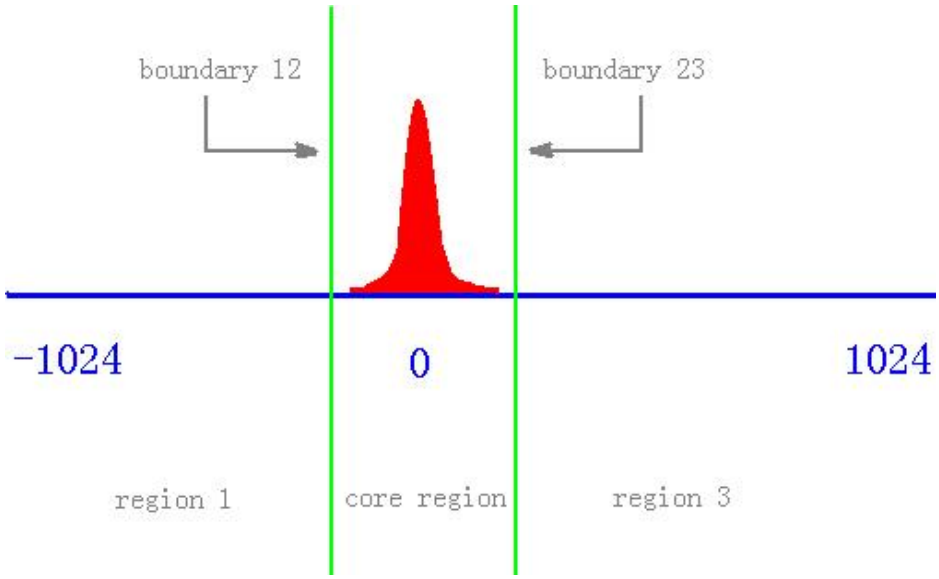

Figure 3.31: The space spans from -1024 a.u. to 1024 a.u. We divided the space into three regions from the left region 1, core region (also region2), region 3. The core region is 25 a.u. wide.

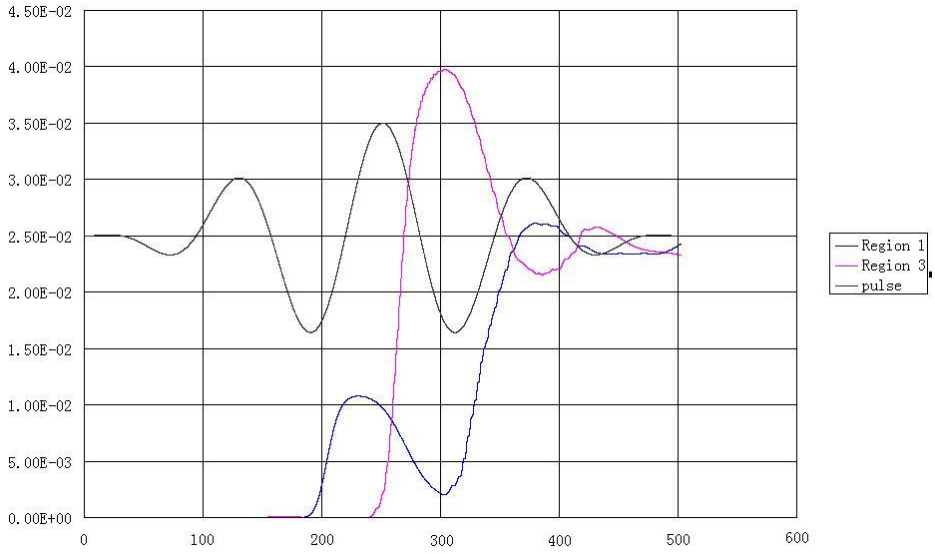

Figure 3.32: The x-axis is time in atomic unit. The vertical axis represents population. We plot the pulse (dark line) in order to take it as reference.

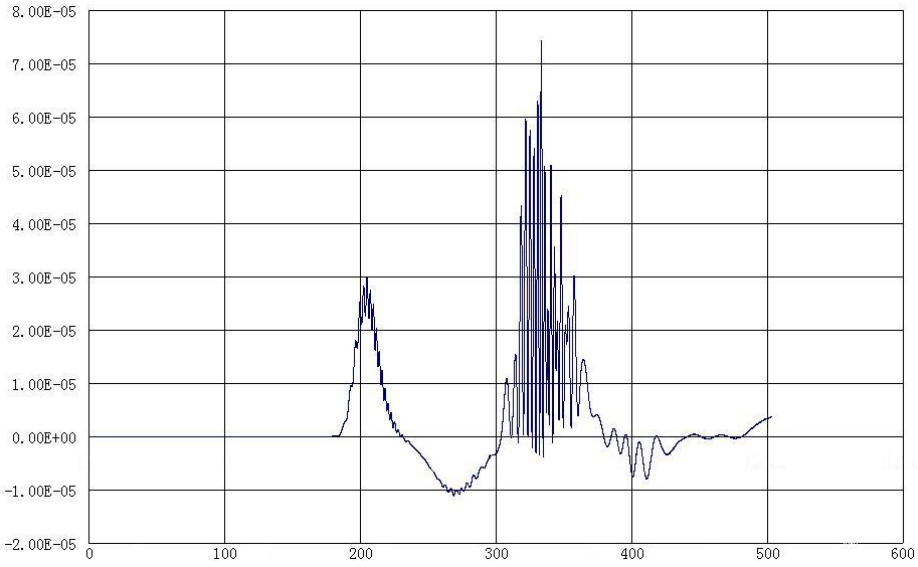

Figure 3.33: The x-axis is time in atomic unit. The vertical axis is relative current intensity.

We plot the population change as a function of time in Figure 3.32. It is clear that most ionization occurs at the central peak of the laser pulse. Re-scattering will occur at the subsequent valley of the pulse. We plot the probability current flow through boundary 12 as a function of time in Figure 3.33. In the region $230 < t < 300$, the negative probability current is an evidence of the re-scattering process. This process is particularly important for the understanding of high harmonic generation process. We will study this process in the future.

3.6 Model H_2^+ ion

In this section we will study a two-center binding potential given by

$$\hat{V}_a(x;R) = -\frac{q}{\sqrt{1+(x+\frac{R}{2})^2}} - \frac{q}{\sqrt{1+(x-\frac{R}{2})^2}}. \tag{3.13}$$

This potential can be viewed as a 1-D H_2^+ ion with two nuclei being clamped. The model is shown schematically in Figure 3.34. The parameter q is added because we want to have

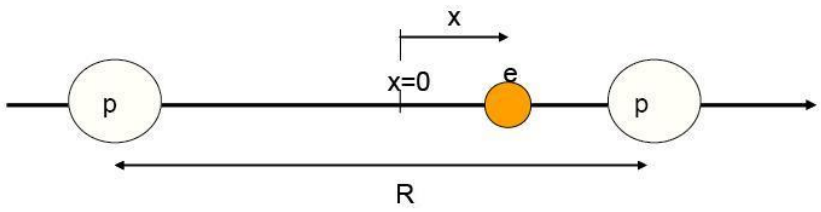

Figure 3.34: A schematic diagram for the H_2^+ ion. The nucleus is clamped at $\pm\frac{R}{2}$; therefore, we only have one degree of freedom.

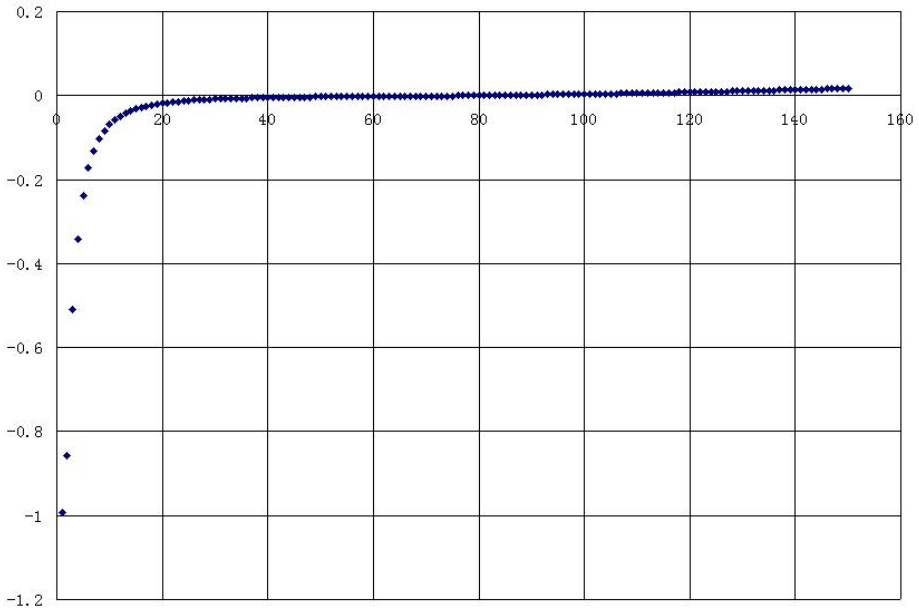

Figure 3.35: We plot the first 150 eigenstates of the potential (3.13). Similar to the atomic case, the bound states have discrete energy levels. The continuous states have positive energy levels and are sufficiently close to each other so that they can be used as bases for photoelectron spectra.

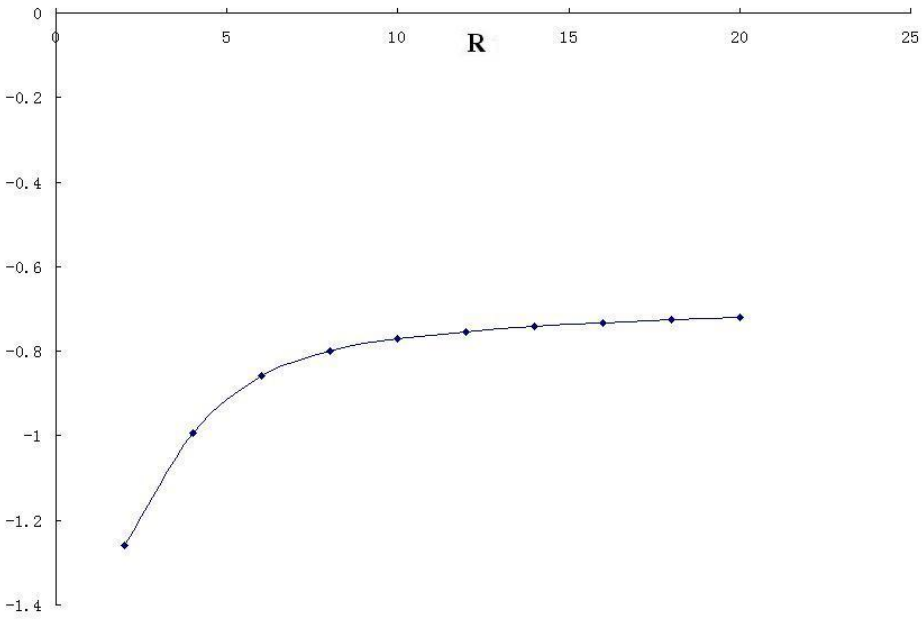

Figure 3.36: Above diagram shows the variation of ground state energy as a function of internuclear separation. We do not include the nuclear repulsion term in the Hamiltonian.

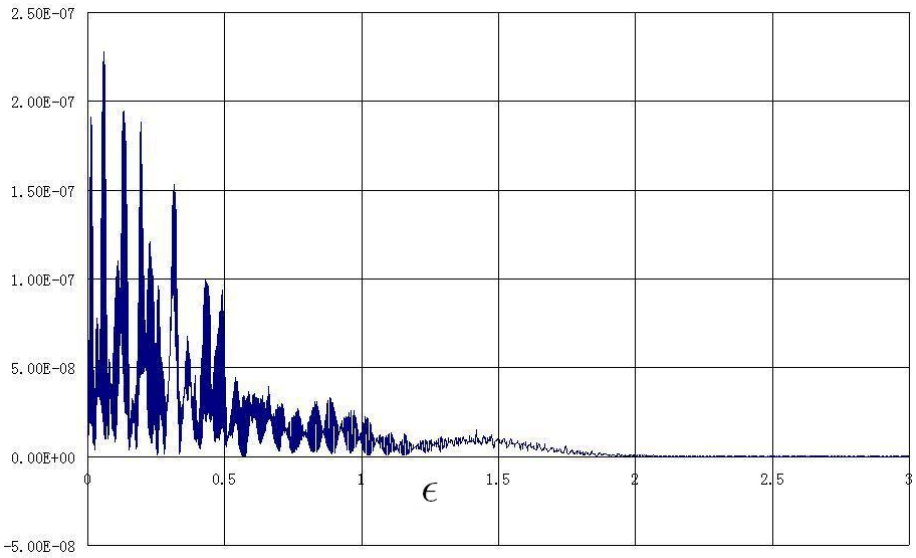

Figure 3.37: PES of 4 cycle sine-square envelope pulse ionization of molecular ion. $E_0 = 0.073$, $\omega_L = 0.05$, $\phi = 0$, $R = 2$ and $q = 0.7$.

the flexibility to adjust the ionization potential such that the system becomes comparable to the atomic case. In this thesis q is set equal to one unless stated otherwise. The eigenstates of the electron can be found by using the same method as in the atomic case (see Section 3.2). The energies of the first 150 states are plotted in Figure 3.35. They are non-degenerate and clearly possess the Rydberg series structure. Compared to the atomic case, we have one more physical parameter to vary – the internuclear separation R. The ground state energy as a function of R is plotted in Figure 3.36. Note that we have not included the nuclear repulsion term in the Hamiltonian which would produce a minimum potential energy at the equilibrium separation $R_0 \approx 2$ a.u.

3.6.1 Comparison between H atom and H_2^+ ion

The photoelectron spectra for the hydrogen molecular ion obtained from TDSE calculation are shown in Figures 3.37, 3.38 and 3.39. All of the trends we observed in the atomic ionization process are also observed in molecular ionization. For instance, as the pulse length increase the ATI peaks become sharper (compare Figure 3.37 with Figure

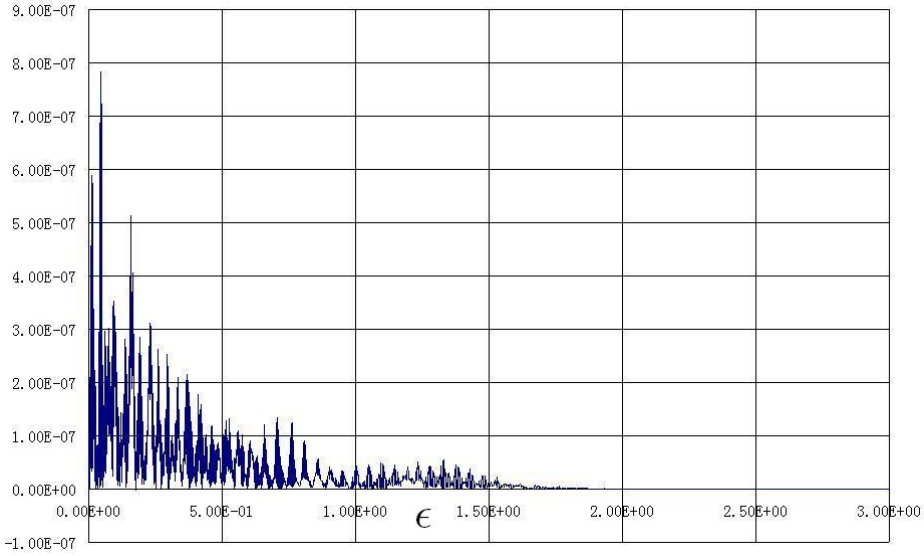

Figure 3.38: PES of 8 cycle sine-square envelope pulse ionization of molecular ion. $E_0 = 0.073$, $\omega_L = 0.05$, $\phi = 0$, $R = 2$ and $q = 0.7$.

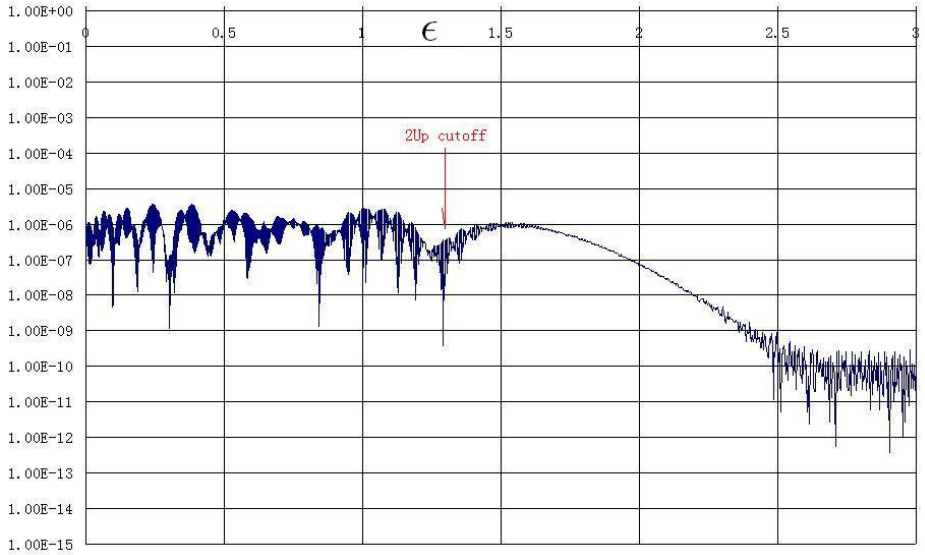

Figure 3.39: In semi-log scale, PES of 4 cycle sine-square envelope pulse ionization of molecular ion. $E_0 = 0.073$, $\omega_L = 0.05$, $\phi = 0$, $R = 4$.

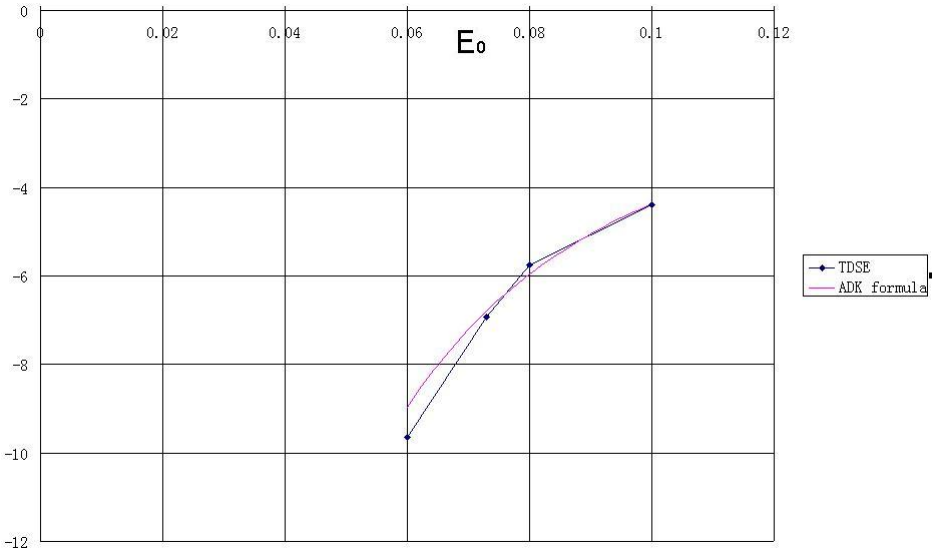

Figure 3.40: Logarithm of total ionization probability versus electric field strength E_0. $\omega_L = 0.05$, $\phi = 0$ and $R = 4$. We take the pre-exponential factor to be $E_0^{-9/2}$ in the ADK formula.

3.38. Here $q = 0.7$ is used because at small internuclear separation we want to have a molecular system that has approximately the same ionization potential as the atomic system.) There is also a direct-electron cutoff located at $2U_p$ (see Figure 3.39, and for the atomic case see Figures 3.13- 3.15). In general, the PES for the molecular ion and for the atom have very similar features. In fact it is difficult to distinguish them by observing the spectra alone.

We plot the total ionization rate as a function of the laser field strength and then fit the TDSE data with ADK formula in Figure 3.40. Since the ADK formula (2.54) (see also eq. B.15) is derived in three dimensions and our model is one-dimensional with a soft-core potential, the pre-factor in ADK formula is unknown. We fit the TDSE calculation by adjusting the exponent of the pre-factor of ADK formula and find $E_0^{-9/2}$ gives the best fit. It is clear the ADK formula describes the trend well.

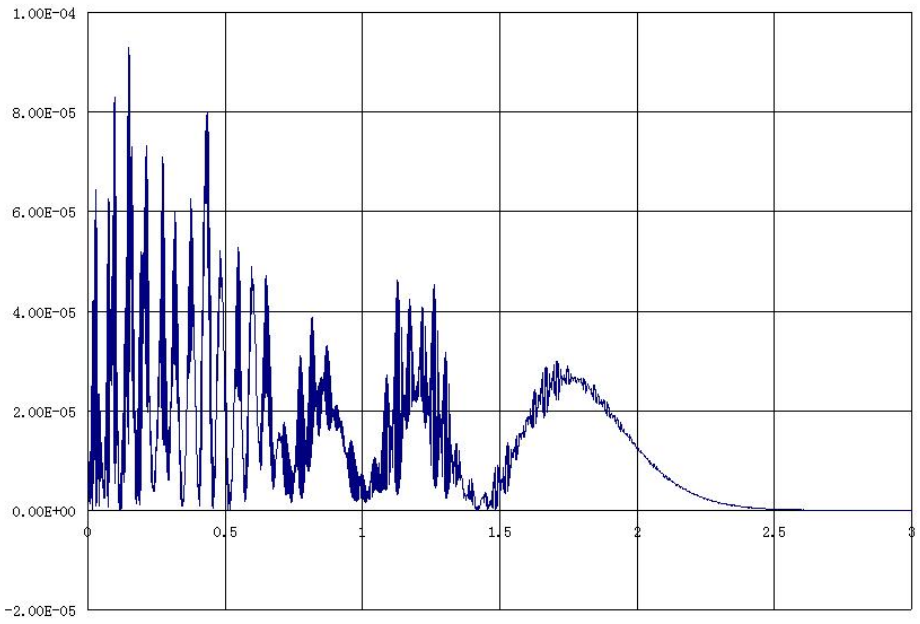

Figure 3.41: PES of 4 cycle sine-square envelope pulse ionization of molecular ion. $E_0 = 0.073$, $\omega_L = 0.05$, $\phi = 0$ and $R = 6$

3.6.2 Dependence on internuclear separation

The PES at $R = 6$ a.u. is plotted in Figure 3.41 and the total ionization rate as a function of internuclear separation is plotted in Figure 3.42. Comparing Figure 3.41 with Figure 3.37, we find that the high energy region of the photo-electron spectrum is greatly enhanced at the moderate internuclear separation of $R = 6$ a.u. From Figure 3.42 where we plot the total ionization rate as a function of separation, we find a maximum also at $R = 6$ a.u. This does not happen by accident. Similar maximum have been observed by Zuo and Bandrauk who explained the phenomena in terms of charge-resonance states [41].

Next we will consider the half-cycle laser ionization spectra shown in Figure 3.43 and 3.44. At small internuclear separation, the spectrum has a single broad peak. As we increase the internuclear separation an interference pattern emerges (See Figure 3.43). In the extreme case when the internuclear separation is 20 a.u, the ion is acting like two hydrogen atoms except the outgoing electron flux will interfere in the way similar to a double slits experiment (See Figure 3.44).

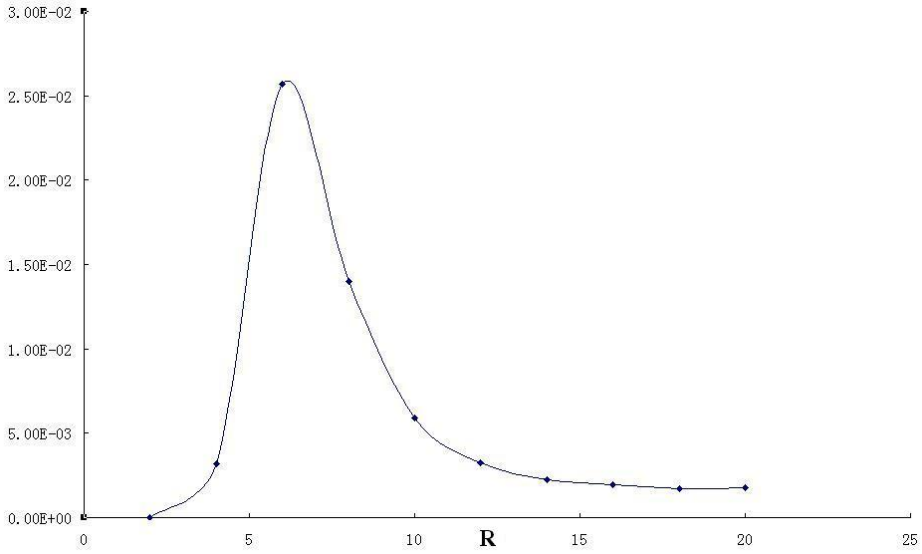

Figure 3.42: Total ionization rate versus internuclear separation. $\omega_L = 0.05$, $\phi = 0$, $E_0 = 0.08$.

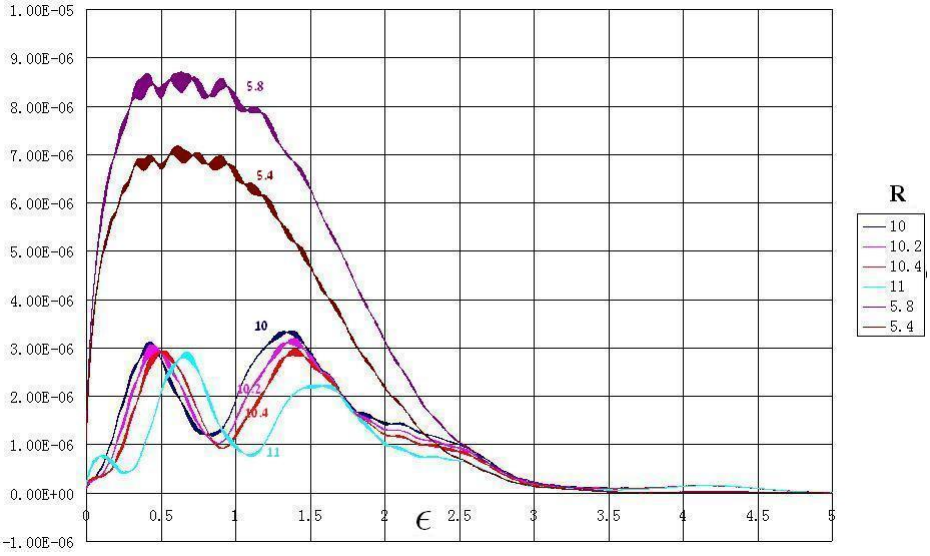

Figure 3.43: PES of a half cycle laser ionization. $\omega_L = 0.05$, $\phi = 0$, $E_0 = 0.073$. The inter-nuclear separation is labeled by color.

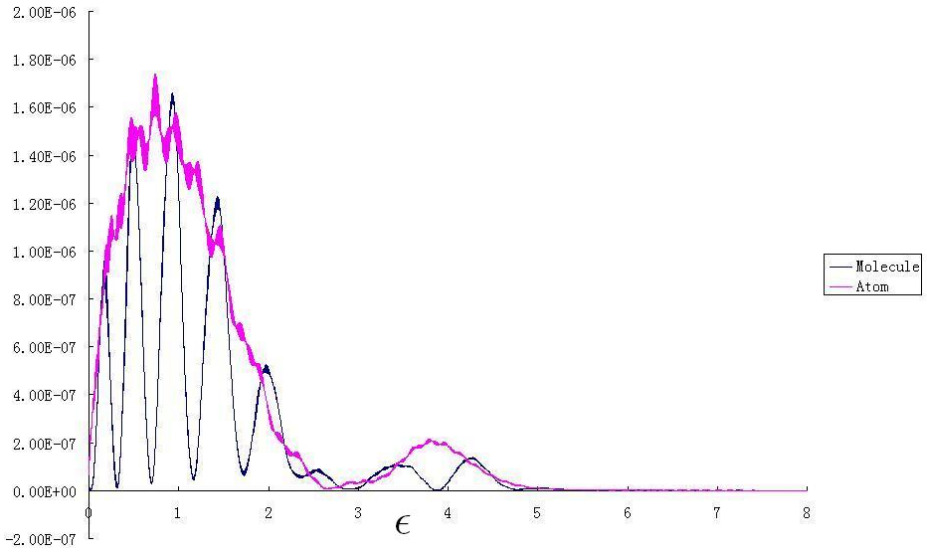

Figure 3.44: PES of a half cycle laser pulse ionization. The $R = 20$ for molecular ion. $\omega_L = 0.05$ $\phi = 0$ $E_0 = 0.073$. The PES of atom is multiplied by a factor of 2.

In addition, we notice even in the half cycle pulse case, ionization is maximum at the moderate internuclear separation (near $R = 6$ a.u.). There are mainly two factors competing each other and one tends to increase the ionization probability and the other tends to decrease the ionization probability. In our case we found as we increase the internuclear separation the ionization potential decreases (see Figure 3.36). This implies the electron becomes more and more loosely bound. The decreasing of ionization potential is one factor that tends to increase the ionization probability. On the other hand, as we increase the internuclear separation the central barrier gets taller and wider so that it impedes the electron tunneling from one core to another (see Figure 3.45). In another words, the electron will have much less mobility at large internuclear separation. It will be trapped within one core. As a result, the bounded electron energy is lowered and the ionization is suppressed. Both factors will contribute to the ionization rate. Only at the optimal internuclear separation the ionization rate will reach maximum.

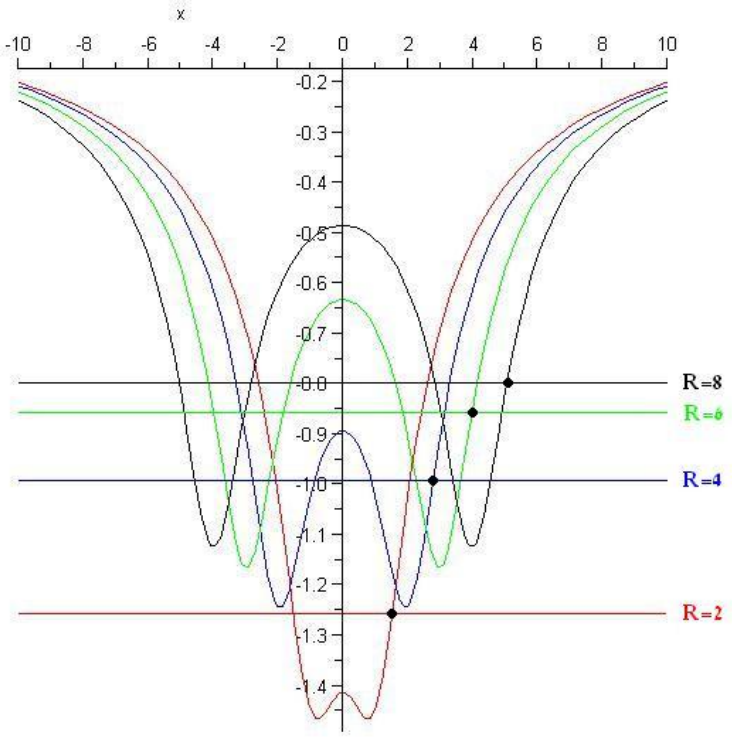

Figure 3.45: The above diagram shows the change of binding potential as internuclear separation changes. The horizontal lines are the corresponding ground state energy levels.

Chapter 4

Conclusion

In this thesis, we have studied the ionization processes of the model H atom and molecular H_2^+ ion. By using these models, we demonstrate the dependence of ionization on various laser parameters. The laser band width will directly affect the width of the ATI peaks in the photoelectron spectra (PES), and the laser intensity is shown to be related to the cutoff of the PES. It is also shown that the CEP becomes significant for ionization by ultrashort laser pulse of only a few cycles. The high energy regions of the PES are sensitive to the CEP, especially for the laser pulse with a square envelope.

Secondly, we have compared SFA calculations with TDSE calculations by varying the physical parameters. The long range nature of the Coulomb field is the main reason for SFA becoming inappropriate. In general, the SFA tends to underestimate the high energy region of the spectra. We believe there are two effects that mainly contribute to this deviation. One is the polarization effect and the other is the re-scattering effect. These two effects are both neglected in the SFA calculation and indeed, are important for the ionization from a Coulomb potential. We show that if the Coulomb tail is screened then the spectra from SFA and TDSE calculations will match very well.

The study of the probability current and population variation indicates that most of the electrons are ionized near the central peak of the short laser pulse and re-scattering will occur subsequently. This shows that the electron dynamics can be controlled by an intense short laser pulse.

In the case of H_2^+ ion, we show that the total ionization probability reaches maximum

at internuclear separation $R \approx 6$ a.u. At this internuclear separation, the high energy region of PES is also greatly enhanced. One reason for this is that as the internuclear separation increases, the central barrier will become taller and wider. At this critical internuclear distance, the central barrier is still low such that electron can tunnel through from one core to the other. At the same time, the ionization potential has been lowered so that the ionization probability is enhanced.

We have also studied atomic and molecular ionization by a half cycle laser pulse. For H_2^+, we find that at large internuclear separation, a half cycle laser pulse will generate electron waves which interfere in a way similar to a double-slit experiment.

In the future, we will study the ionization of H_2^+ ion more in detail. We expect to find a rigorous explanation of the ionization enhancement. The SFA calculation of H_2^+ ion will also be carried out and compared with the TDSE calculation. The problem of gauge dependency in SFA calculation particularly interests me because through the study we gain deep insight of quantum mechanics.

Appendix A

Atomic units

In order to change SI units to atomic units we should see how much degree of freedom the system has. This can be achieved by looking at the dimensionless fine structure constant,

$$\alpha = \frac{e^2}{4\pi\epsilon_0}\frac{1}{\hbar c}.$$

Since fine structure constant is not equal to one, we can only set any three constants out of four equal to one. Conventionally, we set the numerical values of $e = 1$, $4\pi\epsilon_0 = 1$ and $\hbar = 1$. The mass of electron m_e is a fundamental constant so we can also set m_e equal to one. Thus the speed of light is equal to the inverse of fine structure constant:

$$c = \frac{1}{\alpha}.$$

Consequently, we can obtain the electric permittivity of free space and magnetic permeability of free space.

$$\epsilon_0 = \frac{1}{4\pi}$$
$$\mu_0 = 4\pi\alpha^2.$$

Now we have enough information to rewrite the Maxwell's equations and Schrödinger equation in atomic units. Simply replace all the constants appear in the equations, we

obtain the Maxwell's equations in atomic units:

$$\nabla \cdot \vec{E} = 4\pi\rho \tag{A.1}$$

$$\nabla \cdot \vec{B} = 0 \tag{A.2}$$

$$\nabla \times \vec{E} = -\frac{\partial}{\partial t}\vec{B} \tag{A.3}$$

$$\nabla \times \vec{B} = 4\pi\alpha^2 \vec{j} + \alpha^2 \frac{\partial}{\partial t}\vec{E}. \tag{A.4}$$

The Schrödinger equations (2.10) and (2.12) become, respectively,

$$i\frac{\partial}{\partial t}\Psi^v = \left[\frac{1}{2}\hat{P}^2 + \vec{A}(t)\cdot\hat{P}\right]\Psi^v + V_a(\vec{r})\Psi^v, \tag{A.5}$$

$$i\frac{\partial}{\partial t}\Psi^\ell = \left[\frac{1}{2}\hat{P}^2 + \vec{r}\cdot\vec{E}(t)\right]\Psi^\ell + V_a(\vec{r})\Psi^\ell. \tag{A.6}$$

In the following table we list some fundamental atomic units.

Atomic unit for mass m_e	m_e	$9.109\times10^{-31} kg$
Atomic unit for angular momentum $\hbar$	$\hbar$	$1.054\times10^{-34} kg\cdot m^2/s$
Atomic unit for charge e	e	$1.602\times10^{-19} C$
Atomic unit for length a_0	$\left[\hbar^2 e^2\right]\left[4\pi\epsilon_0 m_e\right]^{-1}$	$0.592\times10^{-10} m$
Atomic unit for time τ_0	$\left[4\pi\epsilon_0\hbar a_0\right]\left[e^2\right]^{-1}$	$2.419\times10^{-17} s$
Atomic unit for energy $\wp_0$	$\left[e^2\right]\left[4\pi\epsilon_0 a_0\right]^{-1}$	$4.360\times10^{-18} J$

Appendix B

Tunneling ionization of hydrogen atom

Consider a hydrogen atom present in a spatial homogeneous static electric field. The electric field is along positive z direction. We can write the Schrödinger equation for this system:

$$\left[-\frac{1}{2}\nabla^2 - \frac{1}{r} + zE(t)\right]\Psi = \varepsilon\Psi \tag{B.1}$$

This above equation is separable in parabolic coordinate system:

$$\begin{aligned} x &= \sqrt{\xi\eta}\cos\phi \\ y &= \sqrt{\xi\eta}\sin\phi \\ z &= \frac{1}{2}(\xi - \eta) \\ r &= \frac{1}{2}(\xi + \eta) \end{aligned} \tag{B.2}$$

The equation B.1 in parabolic coordinates takes the following form:

$$\begin{aligned} \varepsilon\Psi \;=\; & \left\{\frac{2}{\xi+\eta}\left[\frac{\partial}{\partial\xi}(\xi\frac{\partial}{\partial\xi}) + \frac{\partial}{\partial\eta}(\eta\frac{\partial}{\partial\eta})\right]\right. \\ & \left. -\frac{1}{2\xi\eta}\frac{\partial^2}{\partial\phi^2} - \frac{2}{\xi+\eta} + \frac{\xi-\eta}{2}E\right\}\Psi \end{aligned} \tag{B.3}$$

The wave function can be written as:

$$\Psi(\xi,\eta,\phi) = f_1(\xi)f_2(\eta)\exp(im\phi) = \frac{\varphi(\xi)\chi(\eta)}{\sqrt{\xi\eta}}\exp(im\phi) \tag{B.4}$$

Substitute the above wave function into equation B.3 we obtained the following equations:

$$\frac{\partial^2}{\partial\xi^2}\varphi(\xi) + \left[\frac{1-m^2}{4\xi^2} + \frac{1+\zeta}{\xi} - \frac{E\xi}{4} + \frac{\epsilon}{2}\right]\varphi(\xi) = 0$$
$$\frac{\partial^2}{\partial\eta^2}\chi(\eta) + \left[\frac{1-m^2}{4\eta^2} - \frac{\zeta}{\eta} + \frac{E\eta}{4} + \frac{\epsilon}{2}\right]\chi(\eta) = 0 \tag{B.5}$$

If we assume initially the hydrogen atom is at ground state and after applying the electric field the atom is still in ground state with energy unchanged then we could obtain the separation constant $\zeta = -\frac{1}{2}$. The magnetic quantum number $m = 0$. Hence the following equations are obtained:

$$\frac{\partial^2}{\partial\xi^2}\varphi(\xi) + \left[\frac{1}{4\xi^2} + \frac{1}{2\xi} - \frac{E\xi}{4} - \frac{1}{4}\right]\varphi(\xi) = 0$$
$$\frac{\partial^2}{\partial\eta^2}\chi(\eta) + \left[\frac{1}{4\eta^2} + \frac{1}{2\eta} + \frac{E\eta}{4} - \frac{1}{4}\right]\chi(\eta) = 0 \tag{B.6}$$

The ground state wave function of hydrogen takes the following form:

$$\Psi(\xi,\eta,\phi) = \frac{1}{\sqrt{\pi}}e^{-\frac{1}{2}(\xi+\eta)} \tag{B.7}$$

Note that in order to go from equation B.5 to equation B.6 we should assume the Coulomb field is very strong in the region close to atomic nucleus so that external electric field can be neglected. Hence we substitute the ground state wave function of hydrogen atom into B.5 to obtain the constants ζ and m. The next step will be using WKB approximation to find the exponential decay factor inside the potential barrier. Here $\varphi(\xi)$ is bounded in all space (see Figure B.1), so it can be approximated by hydrogen ground state wave function. Hence we only need to worry about the wave function $\chi(\eta)$.

Within the potential barrier the wave function has the following form:

$$\chi(\eta) = \frac{C}{\sqrt{|p|}}\exp\left[-\int_{\eta_0}^{\eta}|p|d\eta\right] \tag{B.8}$$

Where p is defined as:

$$p = \sqrt{\frac{1}{4\eta^2} + \frac{1}{2\eta} + \frac{E\eta}{4} - \frac{1}{4}} \tag{B.9}$$

The point η_0 is so chosen such that Coulomb field is very strong and external electric field can be neglected. Hence by matching the boundary condition at this point we can obtain the pre-factor:

$$C = \sqrt{\eta_0}\sqrt{|p(\eta_0)|}e^{-\frac{1}{2}\eta_0} \tag{B.10}$$

. The wave function outside the barrier after tunneling will become:

$$\begin{aligned}\chi(\eta) &= \left\{-\sqrt{\eta_0}\sqrt{|p(\eta_0)|}e^{-\frac{1}{2}\eta_0}\exp\left[-\int_{\eta_0}^{\frac{1}{E}}|p|d\eta\right]\right\} \\ &\quad \frac{1}{\sqrt{p}}\exp\left[i\int_{\frac{1}{E}}^{\eta}pd\eta+\frac{i}{4}\pi\right]\end{aligned} \tag{B.11}$$

The exponential factor inside curly bracket contains an integration over the potential barrier which is approximately from η_0 to the right classical turning point $\eta = \frac{1}{E}$. This factor will responsible for the tunneling ionization rate. In order to evaluate this integral the following approximation is used:

$$|p| \approx \frac{1}{2}\sqrt{1-\frac{2}{\eta}-E\eta} \approx \frac{1}{2}\sqrt{1-E\eta}-\frac{1}{2\eta}(1-E\eta)^{-\frac{1}{2}} \tag{B.12}$$

Because the electric field is alone positive z direction, we expect the ionized electron current will flow in the negative z direction and mostly concentrated near the z axis. In another words, the velocity of the electron in z direction will be much larger than the velocity perpendicular to z direction. Hence we calculate the total ionization rate by summing up the probability flux through an imaginary circular plane that perpendicular to z axis at infinitely far:

$$W_{ion} = \int_0^{2\pi}d\phi\int_0^{\infty}d\rho\rho\vec{j_z} \tag{B.13}$$

Where the probability current is given by:

$$\vec{j_z} = \frac{i}{\pi}\frac{\varphi^2(\xi)}{\eta\xi}\left[\chi(\eta)\frac{d\chi^*(\eta)}{d\eta}-\chi^*(\eta)\frac{d\chi(\eta)}{d\eta}\right] \tag{B.14}$$

Substitute B.11 and use hygrogen wave function for $\varphi(\xi)$ we obtain the tunneling ionization rate for ground state hydrogen atom:

$$W_{ion} = \frac{4}{E}\exp\left(-\frac{2}{3E}\right) \tag{B.15}$$

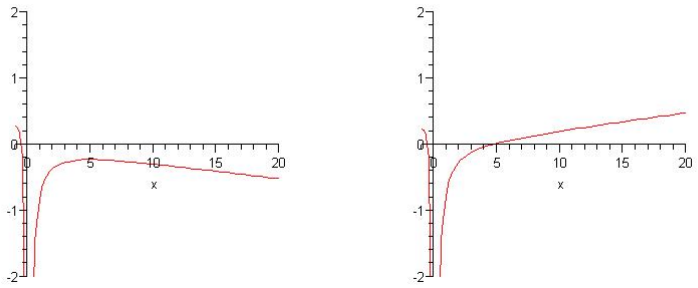

Figure B.1: Effective potentials for equation B.6. The wave function $\varphi(\xi)$ is bounded so it can be approximated by hydrogen ground state (right). The wave function $\chi(\eta)$ is quasi-static. The probability of tunneling through the potential barrier can be calculated by WKB approximation.(left)

For an arbitrary atom instead of using ground state wave function, we can use the asymptotic form of the general hydrogen wave function to match the boundary condition at point η_0. Single active electron approximation is always assumed in this case and the many electron effect is taken into account by effective quantum number[1].

Appendix C

The Volkov state of electron

We start from the Schrödinger equation of a free electron in a spatially homogeneous electric field in the Coulomb gauge, (eq. (2.1) in a.u. with $\hat{V}_a = 0$)

$$i\frac{\partial}{\partial t}\Psi = \frac{1}{2}[-i\nabla + \vec{A}(t)]^2\Psi \tag{C.1}$$

Introduce the Kramers-Henneberger transformation[23]

$$\Psi = \exp\left[-\frac{i}{2}\int^t A(\tau)^2 d\tau\right]\exp[-\nabla\cdot\int^t \vec{A}(\tau)d\tau]\ \psi. \tag{C.2}$$

The new equation becomes the free wave equation

$$i\frac{\partial}{\partial t}\psi = -\frac{1}{2}\nabla^2\psi \tag{C.3}$$

with a plane wave solution. Hence the Volkov solution in the Coulomb gauge is

$$\Psi = \exp\left[i\vec{k}\cdot\vec{r} - i\frac{k^2}{2}t - i\int^t\left(\vec{A}(\tau)\cdot\vec{k} + \frac{1}{2}A^2(\tau)\right)d\tau\right], \tag{C.4}$$

which is the same as eq.(2.14). The Volkov solution in length gauge is given by the gauge transformation (2.6) with $\chi(\vec{r},t) = -\vec{r}\cdot\vec{A}(t)$:

$$\Psi^\ell = \exp\left[i\left(\vec{k} + \vec{A}(t)\right)\cdot\vec{r} - i\frac{k^2}{2}t - i\int^t\left(\vec{A}(\tau)\cdot\vec{k} + \frac{1}{2}A^2(\tau)\right)d\tau\right] \tag{C.5}$$

Notice the time dependent phase factor $\exp[-i\int^{t}\frac{1}{2}A^2(\tau)d\tau]$ give rise to a shift in the total energy. The time average of the energy shift is called the pondermotive potential. This potential corresponds to a quivering energy of the electron which will be returned to the radiation field after the interaction is over.

The canonical momentum of the electron is $\vec{k}$. It is invariant during the interaction. The mechanical momentum is $\vec{k}+\vec{A}(t)$. It is the actual momentum that we measure in the experiment. As we can see the motion of electron in the continuum follows Newton's equation of motion.

Appendix D

Adiabatic approximation

The following equation describes a charged particle in the presence of both atomic potential and electromagnetic radiation

$$i\frac{\partial}{\partial t}\Psi = -\frac{1}{2}\nabla^2\Psi + \hat{V}_a\Psi + \vec{r}\cdot\vec{E}(t)\Psi. \tag{D.1}$$

We want to reduce the equation to the following form:

$$\epsilon(t)\Psi' = -\frac{1}{2}\nabla^2\Psi' + \hat{V}_a\Psi' + \vec{r}\cdot\vec{E}(t)\Psi' \tag{D.2}$$

Now assume at any instant of time we can find eigenfunctions Ψ'_n so that they form a complete and orthogonal basis. Then we can expand the true wave function in terms of these time-varying basis functions.

$$\Psi = \sum_n c_n(t)\Psi'_n \exp\left(-i\int \epsilon_n(t')dt'\right). \tag{D.3}$$

If we substitute the expansion into the original equation, the following system of differential equations can be obtained

$$\dot{c}_m = -\sum_n c_n(t)\exp\left[i\int dt'(\epsilon_m(t') - \epsilon_n(t'))\right]\langle\Psi'_m|\frac{\partial}{\partial t}|\Psi'_n\rangle \tag{D.4}$$

Applying the transformation:

$$c_n = c'_n \exp\left[\int dt'\langle\Psi'_n|\frac{\partial}{\partial t}|\Psi'_n(t')\rangle\right]$$

$$\epsilon'_n(t) = \epsilon_n - i\langle\Psi'_n|\frac{\partial}{\partial t}|\Psi'_n(t')\rangle$$

$$\Psi''_n = \Psi'_n \exp\left[-\int dt'\langle\Psi'_n|\frac{\partial}{\partial t}|\Psi'_n(t')\rangle\right],$$

the system of differential equations become:

$$\dot{c}'_m = -\sum_{n\neq m} c'_n(t)\exp\left[i\int dt'(\epsilon'_m(t') - \epsilon'_n(t'))\right]\langle\Psi''_m|\frac{\partial}{\partial t}|\Psi''_n\rangle. \tag{D.5}$$

The matrix element

$$\left|\langle\Psi''_m|\frac{\partial}{\partial t}|\Psi''_n\rangle\right| = \left|-\frac{\langle\Psi''_m|\partial_{t'}\hat{H}|\Psi''_n\rangle}{\epsilon'_m - \epsilon'_n}\right| \ll 1. \tag{D.6}$$

It is very small because the change of Hamiltonian in time is slow compare with the characteristic frequency of the electron oscillation. The first order approximation is obtained by setting $c'_n(t)$ equal to δ_{ns}, where the subscript s labels the initial state of the wave function and the following solution is obtained.

$$c'_m(t) = \int dt' \frac{\langle\Psi''_m|\partial_{t'}\hat{H}|\Psi''_s\rangle}{\epsilon'_m - \epsilon'_s}\exp\left(i\int dt''(\epsilon'_m - \epsilon'_s)\right)$$

$$c'_s = constant.$$

This solution suggests that if initially the electron is in state s to first order approximation the system will remain in state s as the Hamiltonian changing in time.

Recall in the SFA approach we have the tunneling condition $\frac{\omega_L}{E_0}\sqrt{2I_p} \ll 1$. This can be rewritten as

$$\frac{\omega_L}{2I_p}\frac{E_{atom}}{E_0} \ll 1, \tag{D.7}$$

where the quantity $E_{atom} = (2I_p)^{3/2}$ is defined to be the characteristic electric field strength for a bounded electron. We can see from eq. (D.7) that the tunneling condition is actually a simultaneous fulfillment of two conditions. The first condition is $\frac{\omega_L}{2I_p} \ll 1$, which implies that the adiabatic approximation eq. (D.6). The second condition is $\frac{E_{atom}}{E_0} \approx 1$, which implies the external electric field strength is comparable to the characteristic atomic binding field strength.

Bibliography

[1] V. Ammosov, N. B. Delone, and V. P. Krainov. *Sov. Phys. JETP*, 64:1191, 1986.

[2] S. Augst, D. Strickland, D. D. Meyerhofer, S. L. Chin, and J. H. Eberly. *Phys. Rev. Lett.*, 63:2212, 1989.

[3] D. Bauer, D. B. Milosevic, and W. Becker. *Phys. Rev. A*, 72:023415, 2005.

[4] D. Bauer, D. B. Milosevic, and W. Becker. *Phys. Rev. A*, 72:023415, 2005.

[5] A. Becker and F. H. M. Faisal. *J. Phys. B: At. Mol. Opt. Phys.*, 38:R1, 2005.

[6] Christer Z. Bisgaaed and Lars Bojer Madsen. *Am. J. Phys.*, 72:249, 2003.

[7] B. H. Bransden and C. J. Joachain. *Physics of atoms and molecules*. Prentice Hall, England, 2003.

[8] P. H. Bucksbaum, R. R. Freeman, M. Bashkansky, and T. J. McIlrach. *J. Opt. Soc. Am. B*, 4:760, 1988.

[9] P. B. Corkum. *Phys. Rev. Lett.*, 62:1259, 1989.

[10] D.Bauer, D.B. Milosevic, and W. Becker. *J. Mod. Opt.*, 53:135, 2005.

[11] J. H. Eberly and J. Javanainen. *Phys. Rev. Lett.*, 60:1346, 1988.

[12] F. H. M. Faisal, A. Becker, and J. Muth-Bohm. *Laser Phys.*, 9:115, 1999.

[13] W. G. Greenwood and J. H. Eberly. *Phys. Rev. A*, 43:525, 1991.

[14] G. F. Gribakin and M. Yu. Kuchiev. *Phys. Rev. A*, 55:3760, 1997.

[15] F. A. Ilkov, J. E. Decker, and S. L. Chin. *J. Phys. B: At. Mol. Opt. Phys.*, 25, 1992.

[16] Jiro Itatani, Hiromichi Niikura, and Paul B. Corkum. *Physica Scripta.*, T110:112, 2004.

[17] Misha Yu Ivanov, Michael Spanner, and Olga Smirnova. *J. Mod.Opt.*, 52:165, 2005.

[18] J. D. Jackson. *Classical electrodynamics*. Hamilton Printing company, USA, 1998.

[19] J. Javanainen, J. H. Eberly, and Qi Chang Su. *Phys. Rev. A*, 38:3430, 1988.

[20] L. V. Keldysh. *Sov. Phys. JETP*, 20:1307, 1965.

[21] Thomas Kim Kjeldsen and Lars Bojer Madsen. *J. Phys. B: At. Mol. Opt. Phys.*, 37:2033, 2004.

[22] Thomas Kim Kjeldsen and Lars Bojer Madsen. *Phys. Rev. A*, 71:023411, 2005.

[23] V. P. Krainov, H. R. Reiss, and B. M. Smirnov. *Radiative Processes in Atomic Physics*. John Wiley Publication, New York, New York, 1997.

[24] K. C. Kulander. *Phys. Rev. A*, 38:778, 1988.

[25] L. D. Landau and E. M. Lifshitz. *Quantum mechanics*. Pergamon press, London, 1958.

[26] Jerome Levesque, Jiro Itatani, Dirk Zeidler, Henri Pepin, Jean-Claude Kieffer, P. B. Corkum, and D. M. Villeneuve. *J. Mod. Opt.*, 53:193, 2005.

[27] M. Lewenstein, Ph. Balcou, M. Yu. Ivanov, Anne LHuillier, and P. B. Corkum. *Phys. Rev. A*, 49:2117, 1994.

[28] D. B. Milosevic, G. G. Paulus, D. Bauer, and W. Becker. *J. Phys. B: At. Mol. Opt. Phys.*, 39:R203, 2006.

[29] Agostini P, Fabre F, Mainfray G, Petite G, and Rahman N. *Phys. Rev. Lett.*, 42:1127, 1979.

[30] A. M. Perelomov, V. S. Popov, and M. V. Terentev. *Sov. Phys. JETP*, 23:924, 1965.

[31] B. Piraux, A. L'Huillier, and K. Rzcazewski. *Super- Intense Laser-Atom Physics*. Kluwer Academic, Nethelands, 1993.

[32] A. Scrinzi, M. Yu. Ivanov, R. Kienberger, and D. M. Villeneuve. *J. Phys. B: At. Mol. Opt. Phys.*, 39:R1, 2006.

[33] B. M. Smirnov and M. I. Chibisov. *Sov. Phys. JETP*, 22:585, 1966.

[34] Michael Spanner. *private communication notes*, 2005.

[35] Q. Su and J. H. Eberly. *Phys. Rev. A*, 44:5997, 1991.

[36] Brabec T and Krausz F. *Rev. Mod. Phys.*, 72:545, 2000.

[37] J. E. Decker T.D.G. Walsh F. A. Ilkov and S. L. Chin. *J. Phys. B: At. Mol. Opt. Phys.*, 27:3767, 1994.

[38] X. M. Tong, Z. X. Zhao, and C. D. Lin. *Phys. Rev. Lett.*, 66:033402, 2002.

[39] Liu W-K. *private communication notes*, 2007.

[40] B. Walker, B. Sheehy, K. C. Kulander, and L. F. DiMauro. *Phys. Rev. Lett.*, 77:5031, 1996.

[41] T. Zuo and A. D. Bandrauk. *Phys. Rev. A*, 52:R2511, 1995.